International Journal of Pharmaceutics 671 (2025) 125279

Contents lists available at ScienceDirect

International Journal of Pharmaceutics

journal homepage: www.elsevier.com/locate/ijpharm

# Abiraterone acetate fixed-dosed combinations with ibuprofen-based therapeutic eutectic and deep eutectic solvents

Shaida Panbachi [a,b,c], Josef Beranek [b], Martin Kuentz [c,*]

[a] University of Basel, Department of Pharmaceutical Sciences, Klingelbergstrasse 50, 4056 Basel, Switzerland
[b] Zentiva, k.s., U Kabelovny 130, 102 00 Praha 10, Czech Republic
[c] University of Applied Sciences and Arts Northwest. Switzerland, School of Life Sciences, Institute of Pharma Technology, Hofackerstr. 30, CH-4132 Muttenz, Switzerland

ARTICLE INFO

*Keywords:*
Deep eutectic solvent(s)
Therapeutic deep eutectic solvent(s)
Eutectic mixture(s)
Enabling formulation(s)
Cancer treatment(s)
Novel pharmaceutic(s)

ABSTRACT

In recent years, deep eutectic solvents (DESs) with their outstanding solubilization properties have emerged as strong candidates for oral enabling formulations of poorly soluble drugs. This study explores the use of drug-based therapeutic DESs (THEDESs) to solubilize a poorly soluble compound with the aim of providing a fixed-dose combination of two complementary therapeutic agents. Specifically, potential anticancer effects of ibuprofen (IBU) are harnessed in a novel type of THEDES to dissolve higher amounts of abiraterone acetate (AbAc), an antitumor agent. Four IBU-based combinations were studied: 1:4 M ratio with octanoic acid (OctA), 1:5 with nonanoic acid (NonA), 1:3 with decanoic acid (DeA) or 1:2 with dodecanoic acid (DoA). Fatty acids of different chain lengths were analyzed and discussed considering surface charge densities obtained via quantum chemistry. The THEDESs listed could apparently dissolve AbAc amounts up to 1311.0 ± 125.4 mg/g in IBU:OctA THEDES, 1151.7 ± 22.2 mg/g in IBU:NonA, 1160.4 ± 33.5 mg/g in IBU:DeA, and 231.3 ± 10.7 mg/g in IBU:DoA. *In vitro* dissolution of the simultaneously released drugs reached 37.8 ± 9.0 % to 64.2 ± 1.0 % for IBU and 5.0 ± 3.3 % to 19.4 ± 0.1 % for AbAc. This increased to between 60.4 ± 2.8 % and 79.4 ± 5.0 % of released IBU, and 23.6 ± 1.0 % to 57.3 ± 5.8 % of released AbAc, with 20 % (w/w) Tween 80 added to the formulations. This showed the significant potential of drug-containing THEDESs as solubilizing agents for poorly soluble drugs, in the form of fixed-dose combinations of synergistic APIs.

## 1. Introduction

### 1.1. Deep eutectic solvents as enabling formulations

Deep eutectic solvents (DES) have gained traction in recent years as novel enabling formulations for poorly soluble active pharmaceutical ingredients (APIs) (Abranches & Coutinho, 2023; Palmelund, Eriksen, et al., 2021; Panbachi et al., 2023, 2024). Such APIs often show poor oral bioavailability and require enabling formulations to reach relevant exposure in preclinical species or humans (Kuentz et al., 2021). DESs are prime examples of an enabling formulation approach, as they have been shown to dissolve extraordinary amounts of otherwise poorly soluble compounds (Abranches & Coutinho, 2023; Fourmentin et al., 2021; Jeliński et al., 2019; Z. Li & Lee, 2016; Morrison et al., 2009; Palmelund, Eriksen, et al., 2021; Palmelund et al., 2019; Panbachi et al., 2023, 2024). Pivotal studies on pharmaceutical DES as enabling formulations used the drugs aprepitant (Palmelund, Eriksen, et al., 2021), indomethacin (Panbachi et al., 2023), and venetoclax (Panbachi et al., 2024), where in each case extraordinary solubility improvements were observed; these were 1057-fold for aprepitant, ≈159′000-fold for indomethacin and 118′200-fold for venetoclax, compared to their aqueous solubility. Similar to the work of Palmelund et al. (Palmelund, Eriksen et al., 2021), some studies have also evaluated *in vivo* performance of the DESs revealing enhanced oral bioavailability of the dissolved APIs. Examples of such studies that compared DES-based formulations with crystalline drug include the works of Borase et al. (Borase et al., 2022) documenting a 2.13-fold improvement in the oral bioavailability of chrysin, Gangane et al. (Gangane et al. 2024) reporting 2.91-fold bioavailability enhancement of zileuton, and 2.9-fold advancement of fimasartan bioavailability as reported by Dangre et al. (Dangre et al. 2024). These studies confirm that enhanced solubilization of APIs can translate to elevated oral bioavailability of DES-based formulations.

* Corresponding author.
*E-mail address:* martin.kuentz@fhnw.ch (M. Kuentz).

https://doi.org/10.1016/j.ijpharm.2025.125279
Received 11 October 2024; Received in revised form 24 January 2025; Accepted 24 January 2025
Available online 26 January 2025

A further important characteristic of DESs is their oral tolerability. Although data on oral *in vivo* toxicity of DESs remain rather limited, it is evidenced that DESs are tuneable and can be orally well tolerable (Fourmentin et al., 2021; García et al., 2023; Paiva et al., 2014). The toxicity of DESs is often highly component-dependent (Abranches & Coutinho, 2023; Fourmentin et al., 2021; García et al., 2023; Hayyan et al., 2015; Juneidi et al., 2016) and can vary based on such a components molar ratio (Hayyan et al., 2015). Furthermore, possible synergistic or antagonistic effects can result in different toxicity compared to the individual parent components (Macário et al., 2018). Hence, it has been generally reasoned that the type III DES made of organic hydrogen bond donors and acceptors are most suitable for pharmaceutical applications due to their generally lower oral toxicity (Abdelquader et al., 2023; Abranches & Coutinho, 2023; Fourmentin et al., 2021; Oyoun et al., 2023; Palmelund et al., 2019).

### 1.2. Therapeutic DES approaches for drug delivery

Therapeutic DESs (THEDESs) represent a subcategory of DES-based drug delivery approaches, where the API is incorporated as a constituting component within the DES itself (Abdelquader et al., 2023; Abranches & Coutinho, 2023). THEDESs have been studied as a viable alternative to other bio-enabling formulations to deliver poorly water soluble drugs as a liquid (Abdelquader et al., 2023; Abranches & Coutinho, 2023; Aroso et al., 2016; Rahman et al., 2021; Wolbert et al., 2019). Although not strictly a DES, the marketed topical product EMLA® consisting of a eutectic mixture of lidocaine and prilocaine is one successful example of such therapeutic eutectic formulations, which has shown greater bioavailability in comparison to other marketed topical products of the same APIs (Abdelquader et al., 2023). THEDESs possess great potential as pharmaceutical drug delivery systems, also owed to the potential synergistic effects of the constituting components (Abranches & Coutinho, 2023; Macário et al., 2018). Nowadays THEDESs are often developed for topical and transdermal applications, but few examples of these mixtures have been reported for oral delivery (Abdelquader et al., 2023; Fourmentin et al., 2021; Javed et al., 2024). Therefore, the oral administration route offers novel opportunities for pharmaceutical research on THEDESs.

### 1.3. Ibuprofen-based THEDESs for cancer treatment

THEDESs studied in literature frequently consist of ibuprofen (IBU), due partially to the strong hydrogen-bonding quality of the API (Fourmentin et al., 2021; I et al., 2020; Javed et al., 2024; J. Pereira et al., 2022; C. V. Pereira et al., 2019; Silva et al., 2020; Sun et al., 2020). Non-steroidal anti-inflammatory drugs (NSAIDs) have demonstrated noteworthy therapeutic anti-cancer properties via anti-metastatic and anti-inflammatory effects on cancer cells (Zhao et al., 2017) and have been used in various THEDESs to provide strong cancer treatment candidates (Javed et al., 2024; J. Pereira et al., 2022; C. V. Pereira et al., 2019; Silva et al., 2020; Sun et al., 2020). Using *in vitro* and *in vivo* studies, Silva et al. (Silva et al., 2020) showed that a THEDES consisting of IBU and perillyl alcohol had notable potential as an alternative treatment for colorectal cancer (Silva et al., 2020). Another example reported in literature based on a system of IBU and limonene (molar ratio 1:4) showed synergistic antiproliferative effects on HT29 cancer cell lines, which seems highly promising for further clinical investigation (C. V. Pereira et al., 2019). Other studies demonstrated examples of DES as the liquid basis for nanosuspensions encapsulating nanoparticulate anti-cancer drugs such as doxorubicin, paclitaxel or 7-hydroxycoumarin (Javed et al., 2024; Sun et al., 2020). Even though these systems do not strictly qualify as THEDESs, they were still interesting as pharmaceutical formulations as they showed an enhanced bioavailability (Javed et al., 2024; Sun et al., 2020). To the authors' knowledge, THEDES systems have not been studied previously as solubilizing vehicles for a second poorly soluble drug. This research gap accordingly provided the main aim for the present study to obtain a meaningful fixed-dose combination product based on a THEDES as a solubilizing vehicle.

### 1.4. Abiraterone acetate-loaded IBU-THEDESs for cancer treatment

The examples above show the benefits of applying THEDESs for improved API bioavailability, which may be applied for different clinical indications such as potential anticancer treatments. Combined in a THEDES, the anticancer effects of two components could be more potent due to potential synergy, comparable to synergisms that have been documented in previous literature (Abranches & Coutinho, 2023; Macário et al., 2018). Hence, this study aims at harnessing DESs' extraordinary solubilization capabilities in a THEDES combining a coactive API with a solubilized cancer treatment API. Specifically, four THEDESs based on IBU and fatty acids are presented as strong solubilizers for a poorly soluble API, i.e., abiraterone acetate (AbAc). The formulations are developed to be orally administrable fixed-dose combination cancer treatment products. It is expected that the antitumor effect of the otherwise poorly soluble AbAc, combined with the anti-metastatic and anti-inflammatory effect of the NSAID in the solubilizing THEDES carrier, should provide augmented cancer treatment. This concept is presented visually in Fig. 1. The given fixed dose combination can be also seen as a model because the technical focus of the present work was on how a meaningful fixed dose combination of poorly water-soluble drug(s) could be achieved by means of THEDES formulation technology.

## 2. Methods and materials

### 2.1. Materials

Abiraterone acetate (AbAc), the poorly soluble model drug in this study, was purchased from Aurisco Pharmaceuticals Co., Ltd. (Zhejiang province, China). The API incorporated into the THEDES solubilizer was 99 % racemic (S)-(+)-Ibuprofen (IBU) purchased from ReagentPlus® (Sigma-Aldrich, Steinheim, Germany). The fatty acids featured in the THEDESs were octanoic acid (OctA), nonanoic acid (NonA), decanoic acid (DeA) and dodecanoic acid (DoA), purchased from Sigma-Aldrich (Sigma-Aldrich, Steinheim, Germany). The chromatography buffer components, HPLC-grade acetonitrile (≥99.9 %), ammonium dihydrogen phosphate and phosphoric acid solution for pH adjustments, were all purchased from Sigma-Aldrich (Sigma-Aldrich, Steinheim, Germany). The fed state simulated intestinal fluid (FeSSIF) buffer components, including the sodium chloride, sodium hydroxide pellets and acetic acid were purchased from Alfa Aesar (Thermo Fisher Scientific, Karlsruhe, Germany), whilst the FeSSIF-V2 powder was purchased from Biorelevant (Biorelevant, London, UK). The desiccant phosphorous pentoxide (99 % purity) was procured through Acros Organics (Thermo Fisher Scientific, Karlsruhe, Germany).

### 2.2. Preparation of formulations (THEDESs and THEDESs with surfactant)

The therapeutic eutectic and deep eutectic solvents consisted of IBU with OctA at molar ratio 1:4, NonA at 1:5, DeA at 1:3 and DoA at 1:2. The specific molar ratios were obtained based on the phase diagrams, as described in section 2.3. The raw materials were stored in a desiccator with phosphorous pentoxide as the desiccant (≈ 0 % RH) at room temperature prior to use. The corresponding amounts of both components (batch size 3 g) were weighed into 20 mL clear headspace vials of 22.5 × 75 mm in diameter (Supelco, Sigma-Aldrich, Steinheim, Germany) with magnetic stirring bar (PTFE-coated, cylindrical with pivot ring, L 12 mm, bar diameter 4.5 mm, BRAND®, Sigma-Aldrich, Steinheim, Germany). The mixtures were then purged with nitrogen before the vials were sealed with 20 mm aluminum pressure release seals (with

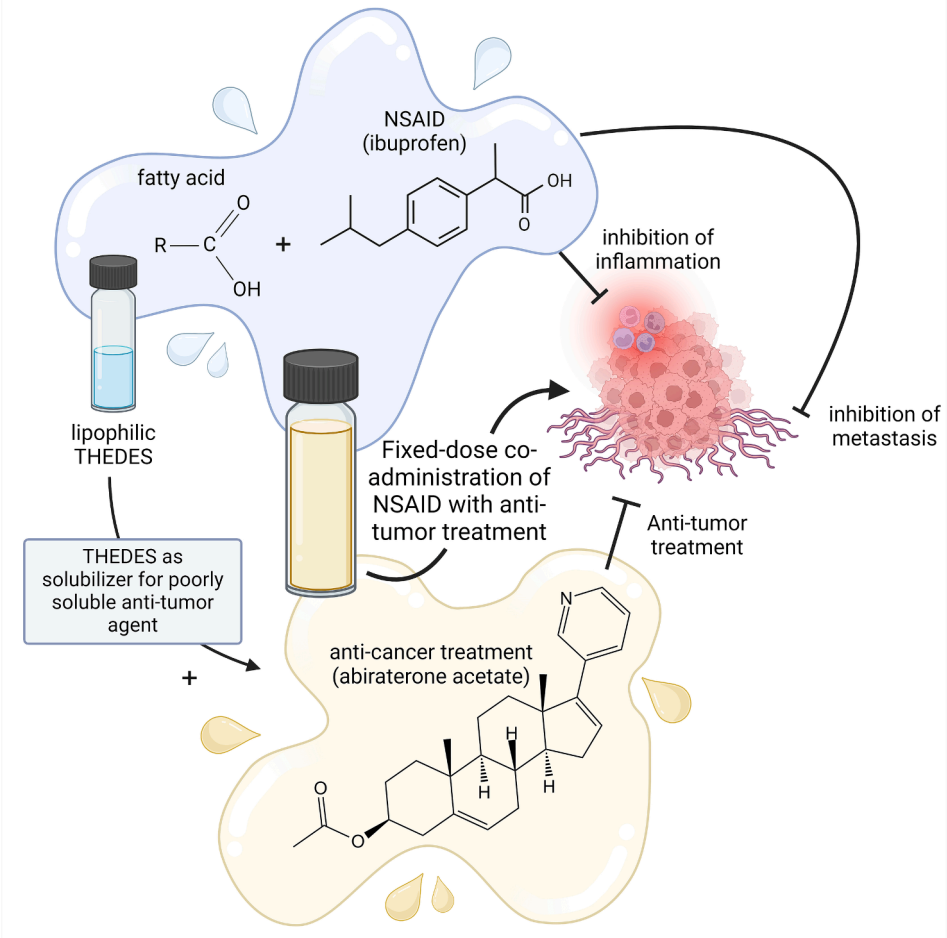


**Fig. 1.** Graphic representation of using the enhanced solubilization capacity of an API-based DES (THEDES) to solubilize a poorly soluble compound with synergistic pharmacological effect as a fixed-dose combination formulation. In this study, an ibuprofen-fatty acid THEDES is developed for solubilization of the antitumor API abiraterone acetate, for possible application as an advanced coactive anticancer treatment.

PTFE/rubber liner, Supelco, Sigma-Aldrich, Steinheim, Germany). The seals were quality-controlled, ensuring that they could not twist. The sealed vials were submerged in a water-filled beaker (150 mL, PYREX®, Thermo Fisher Scientific, Karlsruhe, Germany) on a temperature-controlled stirring-heating plate (IKA® RCT basic, Staufen, Germany). The samples were stirred at 350 rpm at 70 °C for 2 h (Dwamena, 2019). The water bath was used to ensure even heat distribution in the samples. The prepared samples were stored in an oven at a constant temperature of 37 °C. In the case of samples with surfactant (intended for better dispersion), 20 % w/w Tween 80 was added to the THEDESs. The density of Tween 80 was 1.08 g/mL, as reported in the product specification sheet, and the amounts were calculated accordingly.

### 2.3. Determination of eutectic points using phase diagrams

The eutectic points of the IBU:OctA, IBU:NonA, IBU:DeA or IBU:DoA THEDES candidates were found using phase diagrams, plotted with melting point analyses at different molar fractions of the two constituent components (Umerska et al., 2020; Wolbert et al., 2019). Amounts corresponding to 10 mg of the physical mixtures with molar fractions 0:1–1:0 were directly weighed into $T_{zero}$ aluminum pans (TA instruments, Eschborn, Switzerland) and covered with $T_{zero}$ aluminum lids (TA instruments, Eschborn, Switzerland). The samples were exposed to a −10 °C to 85 °C heating ramp at 1 °C/min, with a 50 mL/min nitrogen purge on differential scanning calorimetry (DSC) (Discovery DSC, TA Instruments, Eschborn, Switzerland). The endothermic peaks obtained on the thermograms represented the melting point of a component in excess and the eutectic point of the THEDES. Hence, the melting onset temperature was selected to construct the solid–liquid line (SL-line) of the mixtures (Umerska et al., 2020; Wolbert et al., 2019). The automatically generated thermograms were analyzed in triplicate on the TRIOS software (version 3.1.0.3538), complementary to the Discovery DSC (TA Instruments, Eschborn, Switzerland).

### 2.4. Modelled phase behavior using the Schröder van Laar (SvL) equation

The melting point of each THEDES molar ratio was calculated using the Schröder van Laar equation (Panbachi et al., 2024; Prigogine & Defay, 1954; Umerska et al., 2020). This equation is derived from the Van't Hoff equation (Deiters, 2012) by assuming an ideal thermodynamic binary system (Deiters, 2012; Prigogine & Defay, 1954; Wolbert et al., 2019). Thus, equation (1) describes the liquid–solid phase equilibrium, corresponding to the Schröder van Laar equation if the activity coefficient $\gamma_i$ is unity (Chakraborty et al., 2021; Prigogine & Defay, 1954; Umerska et al., 2020; Wolbert et al., 2019):

$$\ln(\chi_i\gamma_i) = -\frac{\Delta H_i}{R}\left(\frac{1}{T}-\frac{1}{T_{m_i}}\right) \quad (1)$$

The equation includes temperature $T$, melting point $T_{m(i)}$ of a component $i$ based on the molar fraction ($\chi_i$) and the fusion enthalpy ($\Delta H_i$) of component $i$ (Prigogine & Defay, 1954). This equation is applied to both components in selected molar fractions from 0 to 1 in 0.005 increments, resulting in two different SL-lines (Prigogine & Defay, 1954; Umerska et al., 2020; Wolbert et al., 2019). The trendlines of the two SL-

lines were then combined to depict the incremental molar fraction increase of one component from left to right, and the other component from right to left, where the intersection of the two lines provides the eutectic point on the phase diagram (Wolbert et al., 2019).

### 2.5. Sigma surface and sigma profiles of THEDES components

The sigma surface and the sigma profiles of the THEDES components in this study were analyzed using the conductor-like screening model in real solvent (COSMO-RS) (Klamt & Schüürmann, 1993). The COSMO-RS theory makes first use of *ab initio* quantum chemical calculations. Thus, based on the chemical 1D or 2D representation of a molecule, a 3D molecular geometry is calculated by means of Density Functional Theory (DFT) using a Becke-Perdew (Becke, 1988) functional and a triple-zeta valence polarized basis set (TZVP) as level of theory (Schäfer et al., 1994). The molecule is placed in a virtual conductor in the form of a dielectric continuum solvation model; the calculated distribution of the screening charge densities on the molecular surface is called a sigma profile (Klamt, 2018; Mu et al., 2007). The quantum-chemical calculations were based on Turbomole v.7.5 software (Turbomole GmbH), linked to the COSMOtherm program (BIOVIA COSMOquick, Version 2020, Dassault systems, Vélizy-Villacoublay, France) for further calculations and display of sigma surfaces and sigma profiles of the THEDES components investigated.

### 2.6. Apparent solubility of AbAc in THEDESs

An excess amount of AbAc was distributed in the THEDES liquids so that a slight residue of particles could be seen suspended in the test samples. The excess was added to a volume of 3 mL of THEDES in the 20 mL clear headspace vials (22.5 x 75 mm diameter, Supelco, Sigma-Aldrich, Steinheim, Germany) with magnetic stirrers as per section 2.2. The vials were purged with nitrogen and sealed (20 mm aluminum pressure release seals with PTFE/rubber liner, Supelco, Sigma-Aldrich, Steinheim, Germany). After being visually assessed for adequate sealing, the vials were submerged in water baths heated to 37 °C and stirred at 350 rpm for 24 h. 2 mL of the suspensions were collected, suspended in 2 mL safe-lock Eppendorf® tubes (Eppendorf AG, Hamburg, Germany) and centrifuged at 14000 rpm and 37 °C for 30 min (MPW-65R centrifuge, MPW Med. Instruments, Warszawa, Poland) with maximum relative centrifugal force of 20,160 g. The resulting supernatant was transferred to a new set of 2 mL safe-lock Eppendorf® tubes (Eppendorf AG, Hamburg, Germany) and centrifuged again using the same settings (14000 rpm for 30 min, relative centrifugal force of 20,160 g). After the second centrifugation, 100 μL was drawn from the supernatants obtained using a positive displacement pipette (Repetman HandyStep®, Gilson, Villiers-Le-Bel, France) with tip (PD-Tips II, Fischer Scientific, Wertheim, Germany) and diluted with a factor of 1:1000 (v/v) in the mobile phase (described in section 2.8 below). All diluted samples were stirred overnight, after which they were filtered using a 0.45 μm filter (ProFill PA, 0.45 μm, Fisher Scientific, Wertheim, Germany) mounted to 3 mL syringes (Injekt®-F Luer Solo syringe, B. Braun Medical AG, Melsungen, Germany) and filled into amber crimp-top 2 mL HPLC vials (Agilent Technologies Co. Ltd., Beijing, China), sealed with caps (silver, PTFE/silicone septa for 2 mL vials, Agilent Technologies Co. Ltd., Beijing, China) and analyzed using the high-performance liquid chromatography (HPLC) method described below (section 2.8). The three separate sample batches for each THEDES made up a triplicate analysis. The apparent solubility of AbAc in the system was presented as the amount of AbAc (in mg) per amount of THEDES (in g). This was to account for the significant shift in volume that occurred with the higher amounts of AbAc apparently solubilized into the THEDES.

### 2.7. Density of the dispensed liquids

The densities of the THEDESs with API were determined by weighing three 100 μL replicates of three separate batches of supernatant (obtained post-centrifugation as per section 2.6) and dividing the results by the volume. This density measurement was also used for the pure THEDESs, and the THEDESs loaded with 80 % of the apparent solubility value used for dissolution testing. Positive displacement pipettes (Repetman HandyStep®, Gilson, Villiers-Le-Bel, France) with 500 μL pipette tips (PD-Tips II, Fischer Scientific, Wertheim, Germany) were used after 37 °C-storage to avoid cooling of the samples centrifuged at that temperature. The 3 × 100 μL volumes were dispensed into plastic weighing boats (Sigma-Aldrich, Steinheim, Germany) and tared on a scale (Balance XPR205, Mettler Toledo, Melbourne, Australia), to obtain the densities of the formulations prepared for dissolution.

### 2.8. HPLC quantification of AbAc and IBU

The AbAc content in the samples was quantified using HPLC on the Agilent 1100 Series Capillary LC System instrument (Agilent Technologies AG, Basel, Switzerland). The mobile phase consisted of a mixture of 70:30 v/v of acetonitrile to 30 mM ammonium dihydrogen phosphate buffer adjusted to pH 2.00 ± 0.05 using a 50 % dihydrogen phosphate solution. A Charged Surface Hybrid (CSH) C18 stationary phase, of 2.5 μm particle size and 4.6 × 100 mm in dimension, from XSelect® CSH™ (Waters Corporation, Massachusetts, USA) was mounted as the applied HPLC column. The method was set to sustain a temperature of 50 °C in the column at a flowrate of 1 mL/min and an injection volume of 5 μL, with detection at an ultraviolet (UV) wavelength of 255 nm, using Agilent OpenLab software version 3.4 (Agilent Technologies AG, Santa Clara, USA). The retention time obtained was 4.18 ± 0.02 min with a maximum acceptable deviation of 10 % (± 0.42 min) for the samples studied, measured with different buffer batches. The calibration curve was plotted using samples diluted from a stock solution of 1 mg/mL of AbAc in the mobile phase, resulting in a 10-point equidistant concentration series of 0.1–1.0 mg/mL. The lower limit of detection (LoD) on the calibration curve was 0.03 mg/mL, while the lower limit of quantification (LoQ) on the calibration curve was 0.10 mg/mL. These limits were determined according to the ICH Q2(R1) guideline: the LoD was calculated by dividing the standard deviation of the response (the y-intercept) by the slope of the standard curve multiplied by 3.3 and the LoQ was calculated by multiplying the result of the previously described division by 10. Samples were analyzed in triplicate and all calculations and statistical evaluations were based on Microsoft Excel data analysis tool pack (version 2016) and GraphPad Prism software (version 10.0.2), respectively.

For simultaneous detection of IBU and AbAc in the samples collected from the dissolution vessels (described in section 2.10), the HPLC quantification method was adjusted to enable detection at substantially lower concentrations. The injection volume in this method was 30 μL while the calibration curves for both APIs were based on triplicate studies of 10 equidistant concentration points between 0.001 and 0.1 mg/mL. The calculated LoD and LoQ were $9.21 \times 10^{-4}$ mg/mL and $2.79 \times 10^{-3}$ mg/mL for the IBU calibration curve and $8.86 \times 10^{-4}$ mg/mL and $2.68 \times 10^{-3}$ for the AbAc. The IBU was detected at a UV-wavelength of 225 nm with retention time of 2.01 ± 0.01 min, with an acceptable deviation range of 10 %. The resulting chromatograms showing peaks of both APIs could then be used to determine the concentration of both APIs simultaneously.

### 2.9. Droplet diameter of THEDESs in water dispersions

Droplet size on aqueous dispersion was measured by dispensing 200 μL of the AbAc-loaded THEDES samples into 20 mL of demineralized water, resulting in a 1:100 v/v dispersion. The samples were gently shaken manually before evaluation with polarized optical light microscopy (Model DSX10-SZH, Olympus corporation, Tokyo, Japan). The diameters of 10 of the largest visible spherical droplets were measured in 10 different optical fields and used to plot a distribution of a total of 100

droplets per dispersed THEDES. Such selection of largest-size droplets per field of view was meant to provide a robust and fast sampling method for a relative comparison of droplet sizes. Magnifications equivalent to 40 × were used to study the surfactant-free THEDESs whilst a magnification of 100 × was needed to study the surfactant-carrying systems.

### 2.10. USP II dissolution tests

The USP II dissolution test of the surfactant-free and surfactant-containing AbAc-loaded THEDESs evaluated AbAc and IBU release. The test was carried out using a SOTAX® AT7 Smart Semi-Automated dissolution bath (SOTAX Pharmaceutical Testing s.r.o, Prague, Czech Republic), connected to a CP Xtend$^{TM}$ piston pump (SOTAX Pharmaceutical Testing s.r.o, Prague, Czech Republic) and a C615 fraction collector (SOTAX Pharmaceutical Testing s.r.o, Prague, Czech Republic) for offline sample collection in HPLC vials. The dissolution bath was heated to 37 °C and paddle speed set to 100 rpm. The dissolution media in this study was FeSSIF with pH 5.0 (Marques, 2004). The buffer was prepared in 6 L batches for six 900 mL dissolution vessels in the dissolution bath. For 6 L of buffer, 71.22 ± 0.01 g of sodium chloride, 24.24 ± 0.02 g of sodium hydroxide pellets and 49.5 mL of acetic acid were added to 5 L of de-ionized water. The pH was then measured using an automated pH meter (FP20 Mettler Toledo, Melbourne, Australia), and adjusted to 5.00 ± 0.05 with a 2 M sodium hydroxide solution. The remaining empty volume in the vessel was then filled to 6 L with de-ionized water. Lastly, 67.2 ± 0.1 g of FeSSIF-V2 powder (Biorelevant, London, United Kingdom) was added to the buffer, after which the solution was stirred at 300 rpm (≈ 1 h) and heated to 37 °C on a heating plate (IKA® RCT basic, Staufen, Germany). 900 mL of the prepared batch was poured into each of the six dissolution vessels. At time point 0, 1 mL of the IBU-based THEDESs loaded with 80 % of the apparent equilibrium solubility value was dispensed into the vessels. Subsequently, 1.5 mL was collected at time points 2, 5, 10, 15, 20, 25, 30, 45, 60, 90, 120, 150 and 180 min and run through the connected 1.6 μm pore-size filters (25 mm Whatman® GF/A glass microfiber filters, Sigma-Aldrich, Steinheim, Germany), before being poured into HPLC vials (Agilent Technologies Co. Ltd., Beijing, China). After the 3 h USP II analysis, the HPLC vials were sealed with caps (silver, PTFE/silicone septa for 2 mL vials, Agilent Technologies Co. Ltd., Beijing, China) and analyzed using the HPLC method described in section 2.8. The resulting release curves were presented as accumulated percentage of released AbAc and IBU from the total amount of API available in the dispensed volume of the formulation. This study was repeated three times.

### 2.11. X-ray powder diffraction (XRPD) evaluation of dissolution precipitates

The precipitates of the USP II dissolution test were obtained by vacuum filtration of the final dissolution vessel contents through a 0.45 μm pore-size membrane filter (MCE, 47 mm in diameter, Ahlstrom-Munksjö, Helsinki, Finland). They were then scraped off the membrane and placed on XRPD sample holders (PMMA, 25 mm sample reception diameter, Bruker AXS GmbH, Karlsruhe, Germany). The individual APIs, IBU and AbAc, along with the pure DeA and DoA components were analyzed to serve as reference points. The solids were identified according to alignment of the peaks obtained with the diffractogram of the individual components within the formulation.

The XRPD instrument D8 Advance X-Ray Diffraction (Bruker Optics GmbH & Co. KG, Ettlingen, Germany) was used to study the precipitated solids in the dissolution tests. Bragg-Brentano Geometry was applied with a vertical goniometer installed at a height of 150 mm and radius of 280 mm. The Two Theta/Theta couple scans in the range of 2-40° with step size of 0.02° and 0.6 s per step was used. A total of 2324 steps were performed, resulting in a total time of 1502 s. Analysis conditions were set to CuKα radiation (λ = 1.542 Å) with generator settings of 40 kV/40 mA. The primary optics settings were set to 2.5° soller slits, with a fixed slit width of 0.6 mm. The fixed sample illumination area was 10 mm with automatic anti-scatter slits. The sample spin was set to 15 rpm with secondary optics settings of the same 2.5° soller slits with 1D mode detector (LYNXEYE XE-T, Bruker Optics GmbH & Co. KG, Ettlingen, Germany).

### 2.12. Statistical analysis and graphical display

Most statistical analyses in this work were performed using GraphPad Prism (version 10.0.2, GraphPad software, California, USA). F-tests and t-tests were done to statistically compare variance homogeneity and means respectively (Harris, 2010). The initial F-test guided the selection of t-tests with either equal or unequal variance. These tests were performed to compare the calculated ideal eutectic points (SvL eutectic points) with the experimental eutectic points to assess the significance of the difference between the two. The tests were also employed to compare the droplet diameter of the AbAc-loaded THEDESs with and without 20 % w/w Tween 80 to assess the significance of the surfactant impact in each THEDES. The total amounts of quantified API content at the end of the dissolution tests were also compared in the formulations with and without the surfactant. *P*-values below 0.05 resulted in rejection of the null-hypothesis, demonstrating a significant difference among a group of means. One-way ANOVAs with post-hoc Tukey testing were calculated for a multiple comparison of mean AbAc solubility values in the THEDESs. The difference between all means to a single set of THEDES means were performed using the Dunnett test. The ANOVA test was also employed to find the difference amongst the droplet diameters of all THEDESs with and without surfactant, to assess the extent of variation.

Graphs and figures of all experiment results were illustrated using the GraphPad prism program. The figure depicting the study concept (Fig. 1) was illustrated using BioRender (Science Suite Inc., Toronto, Canada) supplied with a license to publish under agreement number IN270813A7. The data analysis tool package on Excel (version 2016, Microsoft Corporation, Washington, USA) was used for linear regression tests (LINEST test) on the calibration curves and estimation of the LoD and LoQs as well as the linear regressions for slope analysis of the drug dissolution experiments.

## 3. Results

### 3.1. Experimental and modeled THEDES eutectic points

The eutectic points of the THEDES samples, based on IBU with either OctA, NonA, DeA or DoA, were found by plotting phase diagrams using the methods described in section 2.3. The phase diagram was designed so that the density of recorded melting points was higher around the suspected eutectic melting point. This was done to ensure better precision of the estimated eutectic point. Fig. 2 shows the phase diagram and SvL model (Equation (1) for comparison for each of the THEDES. Table 1 presents the experimentally obtained lowest recorded melting point as the eutectic point (experimental $T_e$), and the modelled SvL eutectic point (SvL $T_e$). Note that in Table 1, system molar fractions are rounded to one decimal place for simplicity. The calculated molar ratios of the fractions are rounded to the nearest integer, which has been advocated as more representative of the defined molar interactions between components in a DES (Abranches & Coutinho, 2023; Fourmentin et al., 2021). Hence, the final formulations were found to have molar ratios of 1:4 in the IBU:OctA THEDES, 1:5 in the IBU:NonA, 1:3 in the IBU:DeA, and 1:2 in the IBU:DoA system. Statistical comparison found that the experimental eutectic points of the IBU:OctA and IBU:DoA differed significantly from the SvL predicted eutectic points ($p$-value $< 0.0001$ for IBU:OctA and $p$-value $= 0.0005$ for IBU:DoA), while the experimental and SvL eutectic points of the IBU:NonA and IBU:DeA did not ($p$-value $> 0.05$).

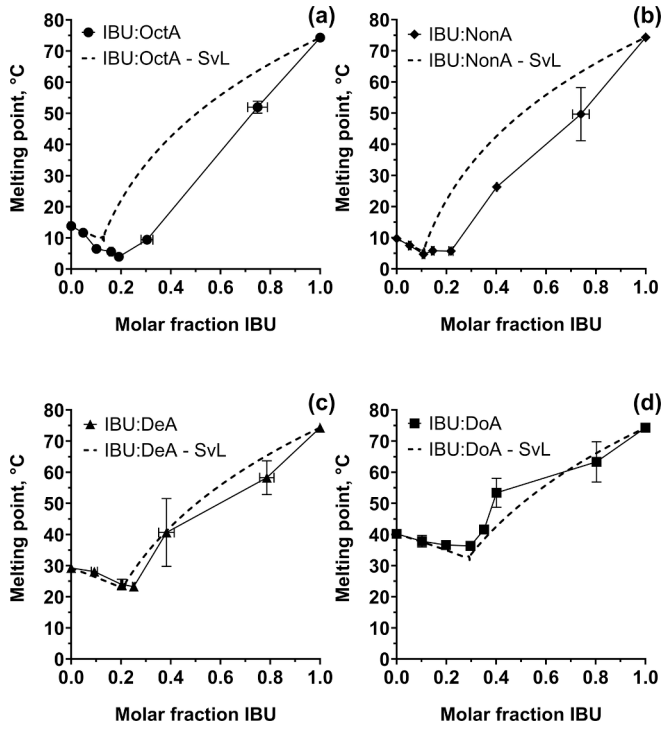


**Fig. 2.** Phase diagrams showing the experimental and Schröder van Laar predicted (SvL) solid–liquid line (SL-line) of the IBU:OctA, IBU:NonA, IBU:DeA, and IBU:DoA THEDES systems (n = 3, mean ± SD). All SvL predicted SL-lines are presented as dashed lines (– – –) in the figures. The experimental SL-line of IBU:OctA is presented in graph (a) as connected lines of round symbols (●), and the IBU:NonA is presented in graph (b) through diamond-shaped symbols (◆), while the IBU:DeA is presented by triangles (▲) in graph (c) and IBU:DoA by squares (■) in graph (d).

**Table 1**
Overview of the Schröder van Laar (SvL) and experimental eutectic points ($T_e$) obtained for each THEDES (n = 3, mean ± SD).

| THEDES | IBU:OctA | IBU:NonA | IBU:DeA | IBU:DoA |
|---|---|---|---|---|
| Experimental $T_e$ | 3.9 ± 0.3 °C | 5.0 ± 0.1 °C | 23.2 ± 0.4 °C | 36.3 ± 0.3 °C |
| Molar fractions at experimental $T_e$ | 0.20:0.80 | 0.15:0.85 | 0.25:0.75 | 0.30:0.70 |
| SvL $T_e$ | 9.4 ± 0.4 °C | 5.5 ± 0.3 °C | 22.8 ± 0.7 °C | 32.3 ± 0.6 °C |
| Molar fractions at SvL $T_e$ | 0.10:0.90 | 0.10:0.90 | 0.20:0.80 | 0.30:0.70 |

### 3.2. Sigma surfaces and profiles of THEDESs

The COSMO-RS model (section 2.5) gave sigma surfaces and sigma profiles of the components studied (IBU, OctA, NonA, DeA, DoA and AbAc) (Figs. 3-4). The molecular structures in Fig. 3 use the ball-and-stick model with standard atom coloring. On the sigma surfaces (Fig. 3, right), clouds of positive screening charge correspond to negatively charged hydrogen-bond accepting regions (marked in red), while the corresponding positively charged hydrogen-bond donating regions are marked in blue, and the neutral regions in green.

The initial sigma surface findings show that the carbon chains of the fatty acids (OctA, NonA, DeA and DoA) differ in length and carry neutral charge. Furthermore, the AbAc molecule is larger, consisting of an acetate prodrug (Ryan & Cheng, 2013), whereas IBU is smaller in comparison. While IBU contributes to the more polar charge density primarily with a single carboxylic acid group, the AbAc molecule has a pyridine group with an electron-rich tertiary nitrogen (Q. Wang et al., 2024) in addition to an ester group. Moreover, a carboxylic acid group was present in IBU and the excipients, which comes with hydrogen-bond donating and accepting tendencies. This is due to the higher positive charge (or corresponding negative screening charge of the sigma profile) of the hydrogen atom in the –OH groups, and the negative charge of the lone electron pairs on the double-bonded oxygen atom (Fourmentin et al., 2021; McMurry, 2015).

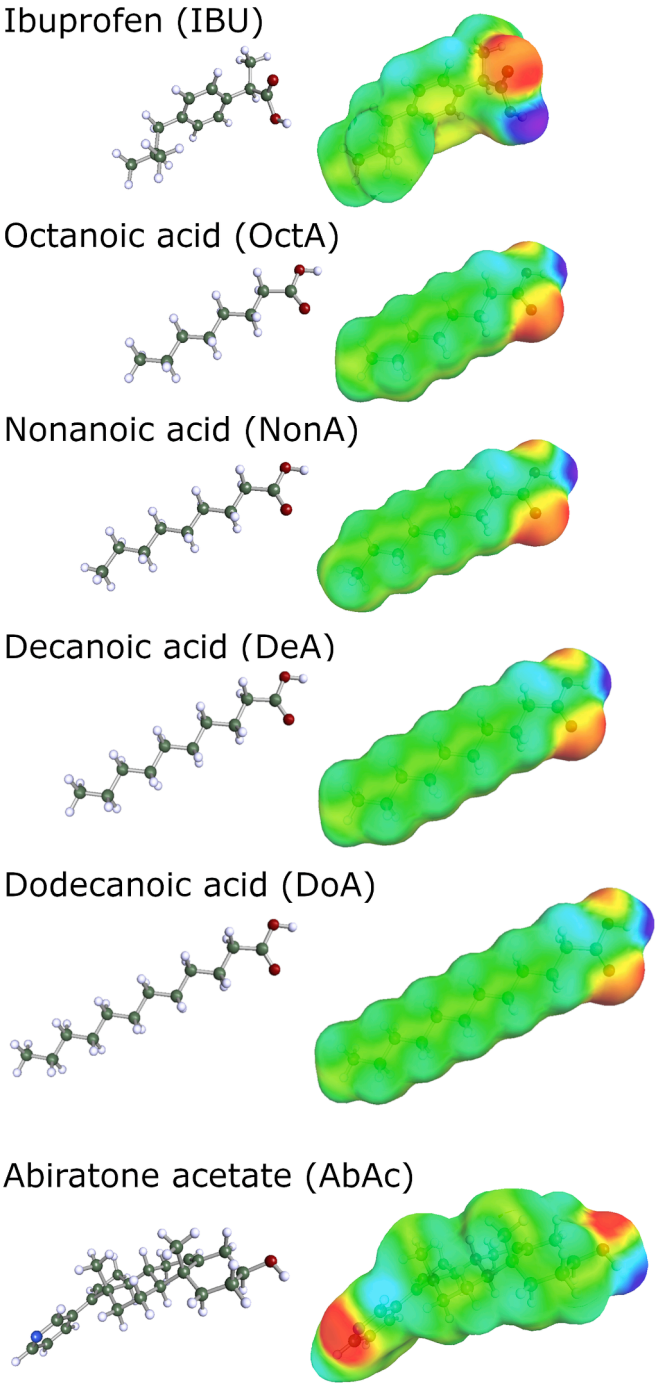


**Fig. 3.** Chemical structures and sigma surfaces calculated using the conductor-like screening model for real solvents (COSMO-RS) of ibuprofen (IBU), octanoic acid (OctA), nonanoic acid (NonA), decanoic acid (DeA), dodecanoic acid (DoA) and abiraterone acetate (AbAc). The molecular structures are presented on the left of the figure, whilst the sigma surfaces are on the right (further details are given in the text).

The sigma profiles obtained from the sigma surfaces are shown in Fig. 4. The x-axis shows the screening charge where hydrogen-bond

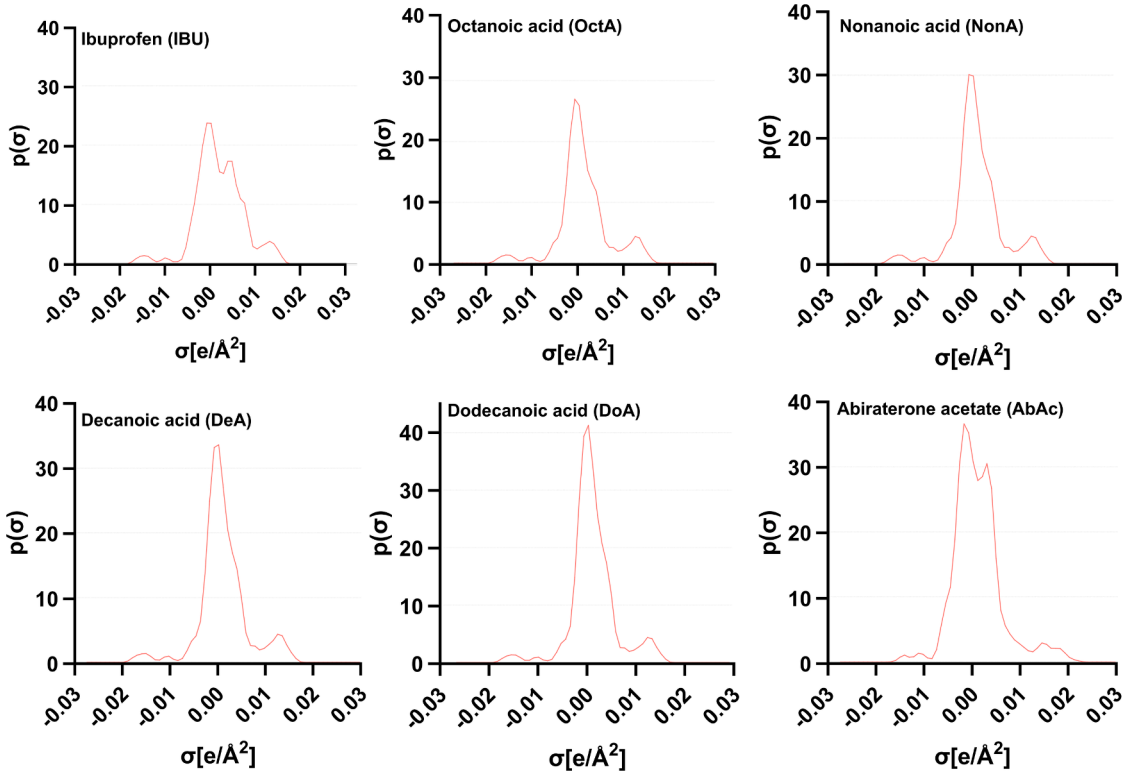


**Fig. 4.** Sigma profiles of ibuprofen (IBU), octanoic acid (OctA), nonanoic acid (NonA), decanoic acid (DeA), dodecanoic acid (DoA) and abiraterone acetate (AbAc) are presented in the graphs above. The x-axis represents the sigma charge density (e/Å$^2$), and the y-axis, the sigma profile (p(σ)).

donating charge densities appear below the sigma-value ($\sigma$) of −0.008 e/Å$^2$, and the hydrogen-bond accepting regions above 0.008 e/Å$^2$ (Mullins et al., 2008; Palmelund et al., 2019). The in-between values represent non-polar regions of the molecules (Mullins et al., 2008; Palmelund et al., 2019). The sigma surfaces of the fatty acids (OctA, NonA, DeA and DoA) do not show significant differences amongst the individual hydrogen bond donating and accepting properties. This was attributed to the carboxylic acid group present in each of the molecules. Nevertheless, a difference in peak height corresponding to the neutral (non-polar) moiety of the molecules is observed. This indicates that with increasing fatty acid carbon chain length, larger areas of the molecules are covered in neutral surface charge.

The sigma surface of the IBU molecule (Fig. 4) also reveals that it consists predominantly of non-polar regions, with smaller peaks linked to the carboxylic acid functional group appearing in the negative and positive regions of the profile. Moreover, despite the presence of an electron-rich tertiary nitrogen in the pyridine of AbAc, the overall hydrogen-bond donating region of the AbAc sigma profile did not seem to differ substantially from the other components. Hence, like IBU, AbAc also consists largely of neutral entities, with the carboxylic acid and the pyridine showing hints of hydrogen bond donating and accepting properties. Although a difference in the intensity of the neutral moieties was observed between the APIs and the fatty acids, the charged regions did not seem noticeably different from those of the fatty acids. Overall, the sigma profiles show that all the molecules in the formulation have carboxylic acids capable of acting as hydrogen bond donors and acceptors, and that differing densities of mainly neutral charge are observed on the molecules.

### 3.3. Apparent solubility of AbAc in THEDESs

To account for the large volume change in the studied samples with AbAc, the solubilities of AbAc were presented per weight of THEDES, by determining the liquid densities of the THEDESs with AbAc. The centrifuged supernatant density of IBU:OctA THEDES (at 37 °C) with AbAc was 1.034 ± 0.005 g/mL, while the supernatant densities of IBU:NonA, IBU:DeA and IBU:DoA THEDES with AbAc were 1.034 ± 0.024 mg/mL, 0.980 ± 0.056 mg/mL and 0.919 ± 0.023 mg/mL, respectively. The resulting apparent solubilities of AbAc in the four THEDESs are listed in Table 2. According to the Tukey test, the solubility of AbAc in the IBU:DoA THEDES was significantly lower than in the other THEDES formulations ($p$-value $< 0.0001$). Although the IBU:OctA THEDES appeared to possess slightly higher AbAc solubility than the IBU:NonA and IBU:DeA systems, they all had similar solubilities with non-significant differences ($p$-value $> 0.05$). Specifically, the Dunnett test of IBU:OctA system resulted in a $p$-value of 0.07 versus IBU:NonA, and 0.09 versus IBU:DeA. Additionally, the difference in means of IBU:NonA and IBU:DeA THEDESs resulted in the $p$-value of 0.998.

The final formulation candidates were loaded with 80 % of the apparent solubility values to ensure that no crystallization could occur because of potential supersaturation during weighing. This resulted in 51.8 % drug loading in the final IBU:OctA formulation (total with API), 48.0 % in the final IBU:NonA, 48.1 % of the total IBU:DeA, and 15.6 % of the total IBU:DoA formulation.

### 3.4. Dispersibility and droplet diameter of formulations in water

The dispersibility of all the prepared THEDESs, with drug-loading corresponding to 80 % of their respective solubilities, was evaluated

**Table 2**
Apparent solubility of AbAc in IBU:OctA, IBU:NonA, IBU:DeA and IBU:DoA THEDESs (n = 3, mean ± SD).

| THEDES, molar ratio of components | Solubility 24 h, 37 °C, $mg_{AbAc}/g_{THEDES}$ |
|---|---|
| IBU:OctA, 1:4 | 1311.0 ± 125.4 |
| IBU:NonA, 1:5 | 1151.7 ± 22.2 |
| IBU:DeA, 1:3 | 1160.4 ± 33.5 |
| IBU:DoA, 1:2 | 231.3 ± 10.7 |

in water to make up oil (THEDES) in water dispersions. The resulting droplet diameters, found via the method described in section 2.9, are summarized in Table 3. To improve dispersibility, 20 % w/w of the surfactant Tween 80 was added to the formulations. This concentration was chosen based on a previous study, where 20 % w/w Tween 80 in a hydrophobic DES improved dispersibility and dissolution without significantly compromising the solubilization capacity of DES in the final formulation (Panbachi et al., 2024). The addition of 20 % surfactant reduced AbAc-loading in the formulations to 41.9 % in IBU:OctA, 38.4 % in IBU:NonA, 38.5 % in IBU:DeA and 12.5 % in IBU:DoA. However, as seen in Table 3, the added surfactant significantly reduces droplet diameters ($p$-value $< 0.0001$), while reducing the degree of variability between the average droplet diameters of the different THEDESs. Overall droplet diameter variability between the different THEDESs was reduced to 6.62 % with 20 % w/w Tween 80, a substantial reduction from the variability without surfactant (47.40 %).

### 3.5. Concurrent USP II dissolution of IBU and AbAc

#### 3.5.1. Release of APIs from AbAc-loaded THEDES

The solubility of IBU in FeSSIF was 297.6 ± 6.6 μg/mL, while the solubility of AbAc in FeSSIF was 147.5 ± 5.1 μg/mL. These values resulted in sink conditions for IBU release and non-sink conditions for AbAc release, from all formulations. According to Fig. 5-a and 5-b, the release of AbAc and IBU from the AbAc-loaded IBU-based THEDES formulations followed identical ranking orders. From highest to lowest, released amounts of AbAc at 180 min were: IBU:NonA 19.4 ± 0.1 % > IBU:DeA 18.9 ± 4.7 % > IBU:OctA 15.5 ± 0.8 % > IBU:DoA 5.0 ± 3.3 %. The same ranking trend follows for 180-min IBU release at 64.2 ± 0.95 % for IBU:NonA, 57.9 ± 6.5 % for IBU:DeA, 47.8 ± 3.4 % for IBU:OctA, and 37.8 ± 9.0 % from the IBU:DoA. Overall, cumulative release of IBU was higher than the AbAc release.

The AbAc release trends from each THEDES resulted in different curves, as given in Fig. 5-a. The release of the IBU:NonA, IBU:DeA and IBU:DoA systems had an S-shape release curve with inflexion point at around 60 min for the IBU:NonA, 90 min for the IBU:DeA and 150 min for the IBU:DoA. At these time points, the amount of AbAc released corresponded to 11.1 ± 1.0 % from IBU:NonA, 7.8 ± 1.3 % from IBU:DeA and 3.7 ± 1.6 % from the IBU:DoA. The slope of the AbAc release curve of IBU:OctA implies a fast release of AbAc at the beginning of the experiment and plateauing after approximately 60 min. At 60 min, 12.1 ± 0.4 % of the AbAc was released from the IBU:OctA system, not much lower than the final release value recorded (15.5 ± 0.8 % at 180 min).

In the early time-points of the experiment (0–45 min), the slope of the IBU release from IBU:DeA THEDES revealed slower release than the one of IBU:OctA (Fig. 5-b). Nonetheless, the ranking was reversed after the 60 min timepoint due to a retardation of the release from the IBU:OctA THEDES. From 0-60 min the amount of IBU released from the IBU:OctA THEDES reached 40.4 ± 2.8 %. However, between 60–180 min, a notable slowing in release quantity was observed. The final cumulative released amount was 47.8 ± 3.4 %, not much higher than the value recorded at 60 min. Furthermore, the overall IBU release of IBU:DeA was slower than IBU:NonA, yet comparable release percentages were observed towards the end of the experiment after 120 min. The amount of IBU released at 120 min was 61.6 ± 0.6 % from IBU:NonA and 54.1 ± 6.6 % from IBU:DeA. In the early minutes of IBU dissolution from IBU:DoA (0–5 min), a spike was observed with released amounts reaching 7.3 ± 1.4 %. This was then followed by a slower gradual release over time, reaching accumulated amounts of 37.8 ± 9.0 %. Ultimately, IBU:DoA showed the least API released by the end of the test run.

**Table 3**
Overview of AbAc-loaded THEDES formulation droplet diameters (THEDES + AbAc) in 1:100 v/v water dispersions, versus droplet diameters of AbAc-loaded THEDES containing 20 % w/w Tween 80 (THEDES + AbAc + 20 % w/w Tween 80) in the 1:100 v/v water dispersions (n = 3, mean ± SD).

| THEDES, molar ratio | THEDES + AbAc | THEDES + AbAc + 20 % w/w Tween 80 |
|---|---|---|
| IBU:OctA, 1:4 | 16.95 ± 8.62 μm | 6.35 ± 0.93 μm |
| IBU:NonA, 1:5 | 17.04 ± 7.54 μm | 6.95 ± 1.45 μm |
| IBU:DeA, 1:3 | 20.83 ± 10.55 μm | 7.37 ± 1.75 μm |
| IBU:DoA, 1:2 | 40.6 ± 25.39 μm | 7.28 ± 1.46 μm |

#### 3.5.2. Release of APIs from surfactant-containing AbAc-loaded THEDESs

The release of the AbAc and IBU APIs increased considerably when Tween 80 surfactant (at a concentration of 20 % w/w) was embedded in the AbAc-loaded THEDES formulations. The enhanced API release is presented as dissolution curves in Fig. 6-a and 6-b. Note that for simplicity, the AbAc-loaded THEDES with 20 % w/w Tween 80 is referred to as surfactant-containing AbAc-loaded THEDES in the text. However, in Fig. 6-a and 6-b the surfactant and its concentration are specified.

Fig. 6-a shows the release ranking (high to low) of AbAc from the four surfactant-containing AbAc-loaded THEDES after 180 min: IBU:DoA at 57.3 ± 5.8 %, followed by IBU:DeA at 38.2 ± 1.3 %, which was on a par with the 37.5 ± 2.0 % from IBU:NonA. These values were significantly higher than the 23.6 ± 1.0 % AbAc recorded from IBU:OctA. The IBU release ranking (Fig. 6-b) after 180 min differed from AbAc, in that the IBU:NonA THEDES system showed the highest release with 79.4 ± 5.0 %, followed by 73.6 ± 0.8 % from the IBU:DeA formulation, then IBU:DoA at 65.1 ± 0.2 % and IBU:OctA at 60.4 ± 2.8 %.

The AbAc release curve of the surfactant-containing IBU:OctA system (Fig. 6-a) exhibited plateauing tendencies after approximately 45 min of dissolution. During this initial period, 10.5 ± 0.4 % of AbAc was released, after which the release stagnated, only reaching 15.5 ± 0.8 % between 45–180 min. Similarly, the release of AbAc from the IBU:DoA system with 20 % w/w Tween 80 in the first 2 min of the dissolution reached 17.9 ± 6.3 %, after which a slower relative release was observed between 2–180 min, reaching 57.3 ± 5.8 %. This value exceeded the quantity of AbAc dissolved from the IBU:OctA formulation with the surfactant.

#### 3.5.3. Effect of surfactant on API-release

The IBU and AbAc content of the THEDES batches tested are listed in Table 4. The cumulative API release values given in Figs. 5-6 are reported as the percentage of API released from the total API content in 1 mL volume of the formulation dispensed into the dissolution vessel. The initial findings of the dissolution tests emphasize a significant rise in the amounts of API released in THEDES with 20 % w/w Tween 80. Fig. 7 provides an overview of the total released amount of the APIs measured at 180 min. These values were compared in pairs to evaluate possible significant differences between THEDESs with and without 20 % w/w Tween in the dissolution media for different drug loads.

### 3.6. Analysis of dissolution test precipitates

The USP II dissolution tests left a solid residue in the form of lumps at the bottom of the dissolution vessels after 180 min. This was seen in all cases except the IBU:DoA formulations with and without 20 % w/w Tween 80. These lumps exhibited a crusty exterior with semi-solid interior. The dissolution test precipitates were extracted using the method described in section 2.11 and the surface of the resulting precipitates was examined using the defined XRPD method. The subsequent diffractograms are presented in Supplementary Figs. 1-4. All formulations except the IBU:DoA showed traces of crystalline AbAc on the surface of the lumps. This was found through the alignment of the X-ray pattern of the lumps aligning with that of crystalline AbAc. In the IBU:OctA systems (with and without 20 % w/w Tween 80), the intensity of the signals was comparable, indicating that both formulations probably had the same level of crystallinity. The diffractogram of the IBU:NonA

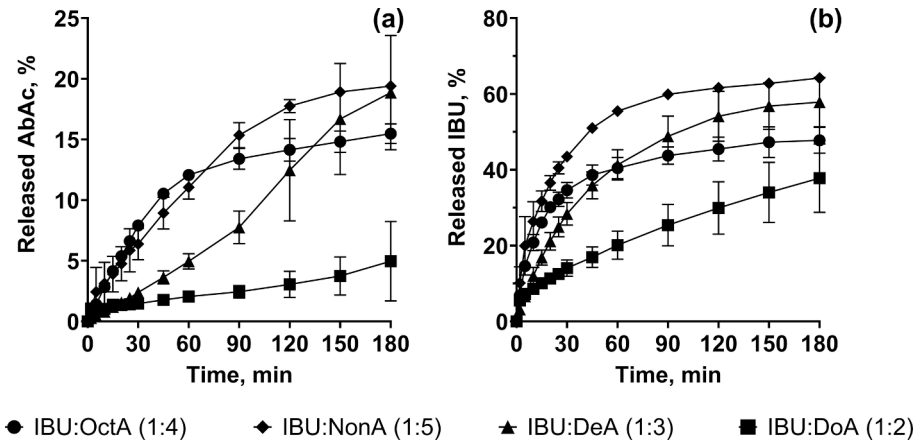


**Fig. 5.** Visual representation of concurrent abiraterone acetate (AbAc) and ibuprofen (IBU) release from the prepared IBU-based THEDESs loaded with AbAc (n = 3, mean ± SD). Graph (a) represents AbAc release from the AbAc-loaded THEDESs, whilst graph (b) shows IBU release. The trend of API release from IBU:OctA is given by connected lines of round symbols (●), IBU:NonA is presented through diamond-shaped symbols (◆), IBU:DeA is presented by triangles (▲) and IBU:DoA by square shaped symbols (■).

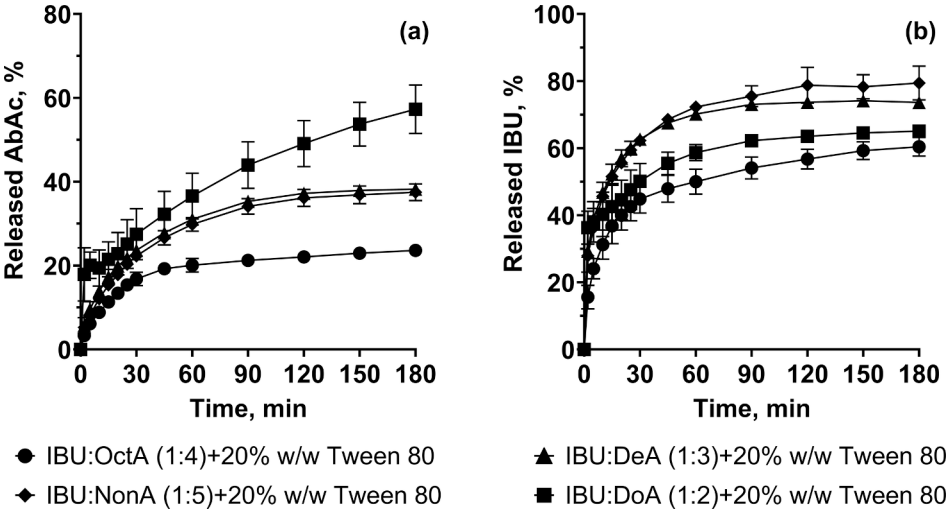


**Fig. 6.** Visual representation of concurrent abiraterone acetate (AbAc) and ibuprofen (IBU) release from the IBU-based THEDESs loaded with AbAc as the poorly soluble API, and 20 % w/w Tween 80 as the surfactant (n = 3, mean ± SD). Graph (a): AbAc release from the AbAc- and Tween 80-loaded THEDESs; Graph (b): IBU release from the formulations. API release from IBU:OctA is shown by round symbols (●), from IBU:NonA by diamond symbols (◆), while the IBU:DeA is presented by triangles (▲) and IBU:DoA by square symbols (■).

**Table 4**
Ibuprofen (IBU) and abiraterone acetate (AbAc) content in 1 mL of the prepared batches of AbAc-loaded THEDES, either with or without 20 % w/w Tween 80 (n = 3, mean ± SD).

| API content in 1 mL dispensed formulation | IBU, mg | AbAc, mg |
|---|---|---|
| IBU:OctA (1:4) | 128.15 ± 2.95 | 519.23 ± 11.95 |
| IBU:OctA (1:4) + 20 % w/w Tween 80 | 106.77 ± 1.56 | 431.73 ± 6.29 |
| IBU:NonA (1:5) | 110.11 ± 2.87 | 490.2 ± 12.76 |
| IBU:NonA (1:5) + 20 % w/w Tween 80 | 87.27 ± 0.48 | 389.01 ± 2.14 |
| IBU:DeA (1:3) | 150.24 ± 3.53 | 488.82 ± 11.49 |
| IBU:DeA (1:3) + 20 % w/w Tween 80 | 117.93 ± 0.57 | 383.7 ± 1.86 |
| IBU:DoA (1:2) | 268.85 ± 13.51 | 146.4 ± 7.36 |
| IBU:DoA (1:2) + 20 % w/w Tween 80 | 219.48 ± 5.04 | 119.48 ± 2.75 |

with 20 % w/w Tween 80 showed slightly stronger signals, which could indicate levels of crystallinity a little higher than compared to the surfactant-free counterpart. Note that Supplementary Figs. 3 and 4 (showing the IBU:DeA and IBU:DoA THEDES diffractograms) include the diffractogram of those fatty acids in the THEDESs that were solid as pure components at room temperature, i.e., DeA and DoA. The IBU:DeA THEDES formulation with 20 % w/w Tween 80 resulted in smaller lumps and sharper peaks in the diffractogram, hence more crystallinity. The diffractograms presented in Supplementary Fig. 4 illustrate that there was no crystalline trace of the APIs, nor of the components, in the IBU:DoA THEDES. This agreed with the absence of solid residue at the bottom of the vessels at the end of the 180 min dissolution test. However, in the case of the IBU:DoA THEDES with surfactant, five sharp peaks were observed with no alignment to the compared profiles. Therefore, the crystalline residue in this sample remained unidentified, with further solid state analysis being outside the scope of the present study aims.

## 4. Discussion

### 4.1. Characterization of THEDESs

The present study describes the pioneering use of THEDESs as a solubilizing vehicle for another drug to obtain a fixed-dose combination product. While fixed-dose combinations generally share the challenge that the fraction of excipients is limited, the current approach harnesses

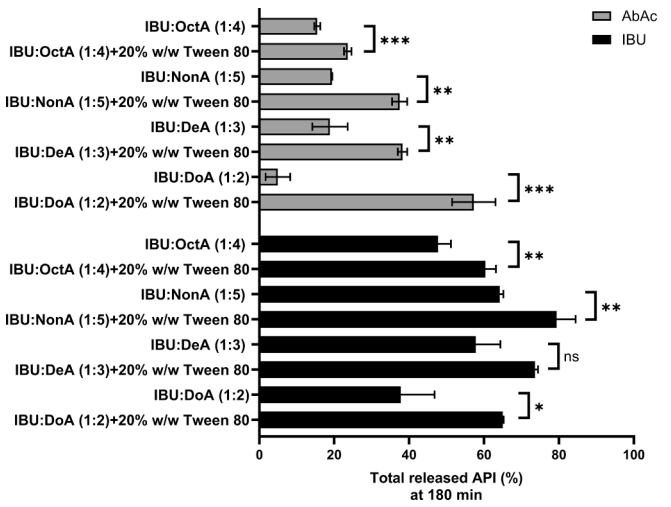


**Fig. 7.** Comparison of total released ibuprofen (IBU) and abiraterone acetate (AbAc) in percent (%) of the total IBU and AbAc in the formulation, after 180 min of dissolution from THEDES (IBU:OctA (1:4), IBU:NonA (1:5), IBU:DeA (1:3), IBU:DoA (1:2)) and THEDESs with 20 % w/w Tween 80 (n = 3, mean ± SD, * represents $p$-values < 0.05, ** $p$-value < 0.01, and *** $p$-value < 0.001 as a level of significance). The gray bars represent the values of AbAc released, and the black represent the values of released IBU.

the solubilizing functionality of one drug to bring the other active compound into a non-crystalline form. Thus, the applicability of four THEDES systems, based on IBU and fatty acids of different alkyl chain length, were studied as enabling solubilizers of the poorly soluble AbAc. The initial step in formulating the four THEDESs was to characterize the thermodynamic behavior of the components. Thus, phase diagrams (section 3.1) were constructed to compare the solid–liquid equilibria of the THEDESs at different molar compositions, as compared to ideal behavior (given by SvL Eq. (1). As the experimentally obtained eutectic point of the IBU:OctA was significantly lower than the corresponding SvL-predicted eutectic point, this THEDES indeed qualified as a DES according to the strict definition put forward by Martins et al. (Martins et al., 2019) (Table 1). In contrast to the IBU:OctA system, the experimental eutectic point of the IBU:DoA system was significantly higher than the SvL-predicted (thermodynamically ideal) eutectic point. This positive deviation in the experimental versus ideal eutectic points of a system appears to be a phenomenon that was observed before in eutectic systems of fatty acids (Abranches & Coutinho, 2023; Crespo et al., 2017). Lastly, the IBU:NonA and IBU:DeA systems could be categorized as simple eutectic systems as no significant deviations between the experimentally observed thermodynamic behavior and thermodynamic ideal conditions were seen.

The aqueous solubility of AbAc was < 0.5 μg/mL according to literature (Solymosi et al., 2018). Hence, the amount of AbAc that can apparently be dissolved in the THEDES (Table 2) was remarkably high, with best case magnitudes reaching more than approximately 400′000-fold solubility increased compared to water. This was in line with the extensive list of DES examples in the literature showing astounding improvements in solubility compared to that in aqueous media (Fourmentin et al., 2021; Huber et al., 2022; Z. Li & Lee, 2016; Lu et al., 2016; Morrison et al., 2009; Palmelund, Eriksen, et al., 2021; Palmelund et al., 2019; Panbachi et al., 2023, 2024). According to the literature, this is due to the distinct polar interactions in a DES that can result in very high solubilization capacities (Abdelquader et al., 2023; Abranches et al., 2020; Palmelund, Rantanen, et al., 2021). The situation may be different in the case of more hydrophobic DES or THEDES; the results of this work revealed that the simple eutectic systems, namely the IBU:NonA and IBU:DeA, only showed a slightly lower solubility compared to that of the 'true' DES, i.e. the IBU:OctA system. Nevertheless, the highly lipophilic API, AbAc, with log P of 5.19 (Hu & Hartmann, 2014) was otherwise expected to dissolve to a greater extent in a more lipophilic system. Hence, if it is assumed that the apolarity of the different THEDESs would increase with the longer fatty acid chains, the IBU:DoA system would outperform THEDESs of shorter alkyl chains. Therefore, the role of the distinct interactions within a DES are emphasized as drivers for improved solubilization of poorly soluble compounds.

### 4.2. *Molecular interactions and impact of fatty acid alkyl chain length in THEDESs*

It is widely assumed that DESs form because of a network of transient interchangeable hydrogen bond interactions (Abranches & Coutinho, 2023; Fourmentin et al., 2021; Martins et al., 2019). It has been speculated that DESs prevalently consist of asymmetric hydrogen bond donors and lone hydrogen bond acceptors (Abranches & Coutinho, 2023). However, it is interesting that here there is only one 'deep' eutectic system in a series of four IBU:fatty acid eutectic systems, all with similar hydrogen bond donating and accepting properties (seen on the sigma profiles, section 3.2). Accordingly, the above mentioned speculation was not supported by the specific systems evaluated in the current study. In the case of the THEDESs with IBU and fatty acids of different carbon chain lengths, sigma profiles of the components did not seem to show marked differences in terms of asymmetry of hydrogen bond donors, nor did they present especially strong cationic clouds in the shape of a lone hydrogen bond acceptor (Abranches & Coutinho, 2023). Alternatively, a shorter fatty acid carbon chain length could result in less of the neutral component (the alkyl chain) on the interacting molecule, which may lead to less steric hindrance of the interacting functional groups on the DES components (Busato et al., 2022). Moreover, studies have suggested that apolar hydrophobic interactions between the components could play a crucial role in the formation of the DES (Busato et al., 2022). Since higher numbers of molecules of the shorter fatty acid chains are interacting with the IBU (1:4 in the IBU:OctA, 1:5 in the IBU:NonA, 1:3 in the IBU:DeA and 1:2 in the IBU:DoA), it is plausible that the prevalence of hydrophobic interactions could be higher, rendering the formulations more likely to form DES. This could contribute to higher free energy of mixing (Goldsack & Chalifoux, 1973), which in turn results in marked eutectic behavior or even DES formation (Abdelquader et al., 2023; Dwamena & Raynie, 2020; S. Li et al., 2024). However, studies have also suggested that the presence of fatty acid hydrogen bond donors with longer alkyl chains contributed to less polarity in a DES, resulting in smaller electron transfers and probably weaker hydrogen bonding (Barani Pour et al., 2024; Dwamena & Raynie, 2020; S. Li et al., 2024). Thus, it appears that the fatty acid alkyl chain length plays an important role in hydrophobic DES formulation through polarity contributions and hydrophobic interactions. Finally, the chain length is expected to affect molecular configurations that directly affect configurational entropy. The latter in turn contributes to the free energy of mixing as a separate driver of DES formation from enthalpic molecular interactions. It is accordingly intriguing to note how comparatively simple formulations from a compositional viewpoint can exhibit complexity on the level of their microstructure.

### 4.3. *Preliminary evaluation of the performance of the novel formulation*

An important aspect of API dissolution from hydrophobic liquid formulations is their ability to disperse in aqueous media (Porter et al., 2008; Pouton, 2006). In this study, the THEDESs prepared with fatty acids of shorter alkyl chains showed smaller droplet sizes when dispersed in water (Table 3), which was attributed to lower lipophilicity (Pouton & Porter, 2008; Rowe et al., 1994). Adding Tween 80 surfactant at a concentration of 20 % w/w caused droplet diameters to shrink even more (Table 3) by further reducing surface tension between the lipophilic oil and the hydrophilic dispersion medium (Porter et al., 2008). Smaller differences were seen among the individual THEDES' droplet

diameters with surfactant compared to variance among surfactant-free THEDES. However, as seen in section 3.5 (Figs. 5-6), smaller droplet diameters did not necessarily result in better API dissolution in the formulations. A mechanistic explanation for this phenomenon is that release rate was affected not only by droplet size and surface area, but also by the drugs' partitioning behavior from hydrophobic vehicle to aqueous bulk solution.

The two APIs showed different release rates from the individual formulations (Figs. 5-6). This was expected due to their different drug lipophilicity as well as different loading concentrations in the formulations, as a result of different IBU:fatty acid molar ratios and different AbAc solubilities. Thus, IBU release was faster and greater overall compared to AbAc release in all formulations (Fig. 7). IBU sink conditions resulted in high partitioning out of the droplets, leaving behind the fatty acid either dissolved or in a separated liquid or solid state in the dissolution medium (depending on the melting point at 37 °C). The slower release of AbAc was the result of higher lipophilicity and consequent non-sink conditions, so that disintegration of the solubilizing carrier (the IBU:fatty acid THEDES) would become critical for release of a hydrophobic drug such as AbAc. In the IBU:OctA samples, a plateauing tendency was observed upon API release. In this case, the fatty acid was a liquid oil at 37 °C (Rowe et al., 1994) as it was the case for the fatty acid in IBU:NonA. However, the release kinetics of the IBU:NonA (in comparison to the IBU:OctA) did not suggest a simple dependence on component polarity. Ultimately, it was reasoned that a given fatty acid incorporated into the individual THEDES formulation had a specific impact on API release behavior, partly due to the drug-specific molar ratio in the mixtures (Koseki et al., 2016).

Nonetheless, lump-shaped precipitates had still formed by the end of all dissolution tests except for the IBU:DoA samples. The precipitated lumps most likely held back the contents of the formulations from extensively partitioning into the aqueous phase. The API covering the surface of the lumps was crystalline AbAc (Supplementary Figs. 1-4), indicating that the kinetics and extent of crystallization was a mechanism to determine drug release. The formation of the crystalline AbAc surface could be due to nucleation and growth of crystals following initial release with supersaturation, or a liquid–liquid phase separation may have occurred at the surface of the droplets because of higher AbAc drug loads (Indulkar et al., 2016). The IBU, being released first (Figs. 5-6), would lead to a loss of solvent capacity in the remaining hydrophobic mixture. Hence adding surfactant (Tween 80) to the THEDESs caused a substantial change in the extent of API release from the formulations, especially in the case of AbAc (Fig. 7). The results demonstrated a positive formulation dispersion effect but there was probably also an effect on drug solubilization in the release medium to sustain higher dissolved API concentrations in the dissolution media (Holm et al., 2023). The dispersion effect was mirrored by the observation of smaller lumps in the case of the IBU:DeA with 20 % w/w Tween 80 compared to surfactant-free lumps. However, this in turn resulted in a higher surface area to volume ratio, which slightly increased crystallinity in the precipitates (Supplementary Fig. 3).

An example of an alternative pharmaceutical formulation approach with similar morphology to the precipitated semi-solids (described above) are so-called liquid marbles, developed as a novel delivery system to increase oral bioavailability (Janská et al., 2019). For this, as well as for the THEDES formulations presented here, the next step would be to study API release and absorption *in vivo*. Especially for hydrophobic liquid formulations, USP II dissolution tests often fall short of mimicking realistic conditions in the lumen of the intestines (Brown et al., 2011). This mainly regards dispersion dynamics in a confined space of large surface area to volume ratio and motility, as in the gastro-intestinal (GI) tract (Brown et al., 2011). Furthermore, it is expected that the fatty acids are readily absorbed in the *in vivo* GI tract (Koseki et al., 2016; T. Y. Wang et al., 2013), further enabling the disintegration of the droplets and facilitating release of the APIs contained in the formulation (T. Y. Wang et al., 2013); this could also not be mirrored in a USP II dissolution setup. However, it is crucial to note that the dissolved APIs reached acceptable amounts, further enhanced by the addition of a surfactant (20 % w/w Tween 80), implying that the dosing requirements could be reduced (Groenland et al., 2021). Furthermore, the application of a fatty-acid based carrier could help reduce the food-effect observed in AbAc administration (Chien et al., 2017; O'Shea et al., 2019).

## 5. Conclusion

This study proposed the concept of using a THEDES as formulation vehicle for another drug to obtain a combination drug product. Thus, a series of four IBU-based THEDESs were developed as solubilizers for the poorly soluble compound AbAc. Initially, phase behavior of the different THEDESs was studied, resulting in eutectic systems of IBU:OctA at the molar ratio of 1:4, IBU:NonA at the molar ratio of 1:5, IBU:DeA at the molar ratio of 1:3, and IBU:DoA at 1:2. Comparison of the experimental eutectic points with the thermodynamically ideal eutectic points (obtained through the SvL model) concluded that the IBU:OctA system reached the pre-requisite of being a 'deep' eutectic solvent (DES), whilst the IBU:DoA system shows similar characteristics to typical fatty acid based eutectic mixtures. The IBU:NonA and IBU:DeA systems were deemed as simple eutectic solvents (Abranches & Coutinho, 2023; Martins et al., 2019). Sigma profiles of the individual components within the systems showed analogous hydrogen bond-donating and accepting functional groups, which still resulted in different thermodynamic phase behavior. Potential contributors were hydrophobic interactions and decreasing polarities with decreasing alkyl chain length of the fatty acids (Busato et al., 2022; Dwamena & Raynie, 2020). This resulted in stronger interactions in the IBU:OctA THEDES system (Abdelquader et al., 2023; Chakraborty et al., 2021; Fourmentin et al., 2021; S. Li et al., 2024) dissolving slightly higher, yet comparable, amounts of AbAc than the IBU:NonA and IBU:DeA (simple eutectic) systems. The AbAc solubility values observed were outstandingly higher than the solubility of AbAc in water. The subsequent simultaneous dissolution of both APIs, the IBU and the AbAc, was characterized using USP II dissolution setups, resulting in adequate levels of released drug, which was further significantly improved with the addition of 20 % w/w Tween 80 to the formulation.

The main aim of the formulations was simultaneous oral delivery of the two APIs, to bring about synergy between the anticancer properties of the two drugs. The uniqueness of this formulation approach is that one of the APIs, namely IBU, functions as a solubilizing excipient for the poorly soluble model drug, AbAc. This is a novel concept that, to the knowledge of the authors, has not yet been explored. This work is the first example of a novel DES-based formulation that may even reduce the pill-burden of cancer patients as one of the advantages of achieving a higher bioavailability (Farrell et al., 2013), thanks to better solubilization of APIs in DESs. Furthermore, it is likely that the food effect of the AbAc may be controlled using this formulation (Chien et al., 2017; O'Shea et al., 2019). Moreover, an improved absorption and synergistic pharmacology with an NSAID could help reducing the currently applied high dose regimens of AbAc (250–1000 mg/day) that are currently still required to treat patients (Attard et al., 2016; Suzuki et al., 2017; Vallet et al., 2020). While the present work had an *in vitro* focus, future work calls on *in vivo* evaluation of the formulations to assess the toxicity and potential synergistic/antagonistic effects (Macário et al., 2018). Finally, the discovery of further THEDESs that can solubilize a poorly soluble API in the form of novel meaningful fixed-dose combinations seems to be a highly attractive research avenue.

## Funding and role of funding source

This work has received funding from the European Union's Horizon 2020 research and innovation program the Marie Skłodowska-Curie grant agreement No 955756. (InPharma). The funding source was not involved in the study design, in the collection, analysis and

interpretation of data, in the writing of the report, nor in the decision to submit the article for publication.

## CRediT authorship contribution statement

**Shaida Panbachi:** Writing – original draft, Visualization, Validation, Project administration, Methodology, Investigation, Formal analysis, Data curation, Conceptualization. **Josef Beranek:** Writing – review & editing, Supervision, Resources, Conceptualization. **Martin Kuentz:** Writing – review & editing, Supervision, Resources, Conceptualization.

## Declaration of competing interest

The authors declare that they have no known competing financial interests or personal relationships that could have appeared to influence the work reported in this paper.

## Acknowledgments

The author would like to thank the invaluable assistance and cooperation of Simona Römerová with the XRPD measurements. Andrew Brown is also acknowledged for his valued proof-reading of the manuscript.

## Appendix A. Supplementary data

Supplementary data to this article can be found online at https://doi.org/10.1016/j.ijpharm.2025.125279.

## Data availability

Data will be made available on request.

## References

Abdelquader, M.M., Li, S., Andrews, G.P., Jones, D.S., 2023. Therapeutic deep eutectic solvents: A comprehensive review of their thermodynamics, microstructure and drug delivery applications. Eur. J. Pharm. Biopharmaceut. 186, 85–104. https://doi.org/10.1016/J.EJPB.2023.03.002.

Abranches, D. O., & Coutinho, J. A. P. (2023). Everything You Wanted to Know about Deep Eutectic Solvents but Were Afraid to Be Told. DOI: 10.1146/annurev-chembioeng.

Abranches, D.O., Martins, R.O., Silva, L.P., Martins, M.A.R., Pinho, S.P., Coutinho, J.A.P., 2020. Liquefying Compounds by Forming Deep Eutectic Solvents: A Case Study for Organic Acids and Alcohols. J. Phys. Chem. B 124 (20), 4174–4184. https://doi.org/10.1021/ACS.JPCB.0C02386/SUPPL_FILE/JP0C02386_SI_001.PDF.

Aroso, I.M., Silva, J.C., Mano, F., Ferreira, A.S.D., Dionísio, M., Sá-Nogueira, I., Barreiros, S., Reis, R.L., Paiva, A., Duarte, A.R.C., 2016. Dissolution enhancement of active pharmaceutical ingredients by therapeutic deep eutectic systems. Eur. J. Pharm. Biopharm. 98, 57–66. https://doi.org/10.1016/J.EJPB.2015.11.002.

Attard, G., Reid, A. H. M., Yap, T. A., Raynaud, F., Dowsett, M., Settatree, S., Barrett, M., Parker, C., Martins, V., Folkerd, E., Clark, J., Cooper, C. S., Kaye, S. B., Dearnaley, D., Lee, G., & de Bono, J. S. (2016). Phase I Clinical Trial of a Selective Inhibitor of CYP17, Abiraterone Acetate, Confirms That Castration-Resistant Prostate Cancer Commonly Remains Hormone Driven. DOI: 10.1200/JCO.2007.15.9749, 26(28), 4563–4571. DOI: 10.1200/JCO.2007.15.9749.

Barani Pour, S., Jahanbin Sardroodi, J., Rastkar Ebrahimzadeh, A., Pazuki, G., & Hadigheh Rezvan, V. (2024). A comparative study of deep eutectic solvents based on fatty acids and the effect of water on their intermolecular interactions. Scientific Reports 2024 14:1, 14(1), 1–18. DOI: 10.1038/s41598-023-50766-1.

Becke, A.D., 1988. Density-functional exchange-energy approximation with correct asymptotic behavior. Phys. Rev. A 38 (6), 3098. https://doi.org/10.1103/PhysRevA.38.3098.

Borase, H.P., Borkar, M.R., Chaturvedi, K.K., Kar Mahapatra, D., Chalikwar, S.S., Dangre, P.V., 2022. Design and evaluation of natural deep eutectic solvents system for chrysin to elicit its solubility, stability, and bioactivity. J. Mol. Liq. 345, 118205. https://doi.org/10.1016/J.MOLLIQ.2021.118205.

Brown, C. K., Friedel, H. D., Barker, A. R., Buhse, L. F., Keitel, S., Cecil, T. L., Kraemer, J., Morris, J. M., Reppas, C., Stickelmeyer, M. P., Yomota, C., & Shah, V. P. (2011). Dissolution/In Vitro Release Testing of Novel/Special Dosage Forms. AAPS PharmSciTech 2011 12:2, 12(2), 782–794. DOI: 10.1208/S12249-011-9634-X.

Busato, M., Mannucci, G., Lisio, V.D., Martinelli, A., Giudice, A.D., Tofoni, A., Bosco, C. D., Migliorati, V., Gentili, A., D'Angelo, P., 2022. Structural Study of a Eutectic Solvent Reveals Hydrophobic Segregation and Lack of Hydrogen Bonding between the Components. ACS Sustain. Chem. Eng. 10 (19), 6337–6345. https://doi.org/10.1021/ACSSUSCHEMENG.2C00920/ASSET/IMAGES/LARGE/SC2C00920_0008.JPEG.

Chakraborty, S., Chormale, J.H., Bansal, A.K., 2021. Deep eutectic systems: An overview of fundamental aspects, current understanding and drug delivery applications. Int. J. Pharm. 610, 121203. https://doi.org/10.1016/J.IJPHARM.2021.121203.

Chien, C., Smith, M., Porre, P.D., 2017. Effect of Food on Abiraterone Pharmacokinetics: A Review. Int. J. Pharmacokinet. 2 (3), 183–193. https://doi.org/10.4155/IPK-2016-0026.

Crespo, E.A., Silva, L.P., Martins, M.A.R., Fernandez, L., Ortega, J., Ferreira, O., Sadowski, G., Held, C., Pinho, S.P., Coutinho, J.A.P., 2017. Characterization and Modeling of the Liquid Phase of Deep Eutectic Solvents Based on Fatty Acids/Alcohols and Choline Chloride. Ind. Eng. Chem. Res. 56 (42), 12192–12202. https://doi.org/10.1021/ACS.IECR.7B02382.

Dangre, P., Avhad, P., Gurumukhi, V., Katolkar, U., Chalikwar, S., 2024. Solidification of deep eutectic solvent containing fimasartan through wet impregnation and exploration of flow attributes by modified SeDeM-SLA expert system. European Journal of Pharmaceutics and Biopharmaceutics 201, 114381. https://doi.org/10.1016/J.EJPB.2024.114381.

Deiters, U.K., 2012. The isothermal van't Hoff equation for phase equilibria—A forgotten relation? Fluid Phase Equilib. 336, 22–27. https://doi.org/10.1016/J.FLUID.2012.08.028.

Dwamena, A.K., Raynie, D.E., 2020. Solvatochromic Parameters of Deep Eutectic Solvents: Effect of Different Carboxylic Acids as Hydrogen Bond Donor. J. Chem. Eng. Data 65 (2), 640–646. https://doi.org/10.1021/ACS.JCED.9B00872.

Dwamena, A. K. (2019). Recent Advances in Hydrophobic Deep Eutectic Solvents for Extraction. Separations 2019, Vol. 6, Page 9, 6(1), 9. DOI: 10.3390/SEPARATIONS6010009.

Farrell, B., French Merkley, V., Ingar, N., 2013. Reducing pill burden and helping with medication awareness to improve adherence. Canadian Pharmacists Journal : CPJ 146 (5), 262. https://doi.org/10.1177/1715163513500208.

Fourmentin, S., Costa Gomes, M., & Lichtfouse, E. (2021). Deep eutectic solvents for medicine, gas solubilization and extraction of natural substances. 312.

Gangane, P., Sahare, A., More, S., Warokar, A., Borkar, M., Dangre, P., 2024. Preparation and impregnation of deep eutectic solvents containing zileuton onto adsorbents to elicit the biopharmaceutical attributes. J. Mol. Struct. 1312, 138655. https://doi.org/10.1016/J.MOLSTRUC.2024.138655.

García, C.B., Concha, J., Culleré, L., Lomba, L., Sangüesa, E., Ribate, M.P., 2023. Has the Toxicity of Therapeutic Deep Eutectic Systems Been Assessed? Applied Sciences (switzerland) 13 (10). https://doi.org/10.3390/APP13105980.

Goldsack, D.E., Chalifoux, R.C., 1973. Contribution of the free energy of mixing of hydrophobic side chains to the stability of the tertiary structure of proteins. J. Theor. Biol. 39 (3), 645–651. https://doi.org/10.1016/0022-5193(73)90075-1.

Groenland, S. L., Ratain, M. J., Chen, L. S., & Gandhi, V. (2021). The Right Dose: From Phase I to Clinical Practice. DOI: 10.1200/EDBK_319567, 41, 92–106. DOI: 10.1200/EDBK_319567.

Harris, D.C., 2010. Mass Spectroscopy | High-Performance Liquid Chromatography. Quantitative Chemical Analysis 565–594. https://www.ebay.co.uk/itm/284475716994.

Hayyan, M., Looi, C.Y., Hayyan, A., Wong, W.F., Hashim, M.A., 2015. In Vitro and In Vivo Toxicity Profiling of Ammonium-Based Deep Eutectic Solvents. PLoS One 10 (2), e0117934. https://doi.org/10.1371/JOURNAL.PONE.0117934.

Holm, R., Kuentz, M., Ilie-Spiridon, A.R., Griffin, B.T., 2023. Lipid based formulations as supersaturating oral delivery systems: From current to future industrial applications. Eur. J. Pharm. Sci. 189, 106556. https://doi.org/10.1016/J.EJPS.2023.106556.

Hu, Q., Hartmann, R.W., 2014. The Renaissance of CYP17 Inhibitors for the Treatment of Prostate Cancer. Cancer Drug Design and Discovery: Second Edition 319–356. https://doi.org/10.1016/B978-0-12-396521-9.00011-5.

Huber, V., Hioe, J., Touraud, D., Kunz, W., 2022. Uncovering the curcumin solubilization ability of selected natural deep eutectic solvents based on quaternary ammonium compounds. J. Mol. Liq. 361, 119661. https://doi.org/10.1016/J.MOLLIQ.2022.119661.

I, B., N, J., Venkatachalam, S., & Datta, D., 2020. A brief review on eutectic mixture and its role in pharmaceutical field. International Journal of Research in Pharmaceutical Sciences 11 (3), 3017–3023. https://doi.org/10.26452/ijrps.v11i3.2398.

Indulkar, A.S., Gao, Y., Raina, S.A., Zhang, G.G.Z., Taylor, L.S., 2016. Exploiting the Phenomenon of Liquid-Liquid Phase Separation for Enhanced and Sustained Membrane Transport of a Poorly Water-Soluble Drug. Mol. Pharm. 13 (6), 2059–2069. https://doi.org/10.1021/ACS.MOLPHARMACEUT.6B00202/ASSET/IMAGES/LARGE/MP-2016-002028_0009.JPEG.

Janská, P., Rychecký, O., Zadražil, A., Štěpánek, F., Čejková, J., 2019. Liquid Oil Marbles: Increasing the Bioavailability of Poorly Water-Soluble Drugs. J. Pharm. Sci. 108 (6), 2136–2142. https://doi.org/10.1016/J.XPHS.2019.01.026.

Javed, S., Mangla, B., Sultan, M.H., Almoshari, Y., Sivadasan, D., Alqahtani, S.S., Madkhali, O.A., Ahsan, W., 2024. Pharmaceutical applications of therapeutic deep eutectic systems (THEDES) in maximising drug delivery. Heliyon 10 (9), e29783. https://doi.org/10.1016/J.HELIYON.2024.E29783.

Jeliński, T., Przybyłek, M., Cysewski, P., 2019. Natural Deep Eutectic Solvents as Agents for Improving Solubility. Stability and Delivery of Curcumin. https://doi.org/10.1007/s11095-019-2643-2.

Juneidi, I., Hayyan, M., Mohd Ali, O., 2016. Toxicity profile of choline chloride-based deep eutectic solvents for fungi and Cyprinus carpio fish. Environ. Sci. Pollut. Res. 23 (8), 7648–7659. https://doi.org/10.1007/S11356-015-6003-4/FIGURES/3.

Klamt, A., 2018. The COSMO and COSMO-RS solvation models. Wiley Interdiscip. Rev.: Comput. Mol. Sci. 8 (1), e1338.

Klamt, A., Schüürmann, G., 1993. COSMO: a new approach to dielectric screening in solvents with explicit expressions for the screening energy and its gradient. J. Chem. Soc. Perkin Trans. 2 (5), 799–805. https://doi.org/10.1039/P29930000799.

Koseki, Y., Ikuta, Y., Kamishima, T., Onodera, T., Oikawa, H., Kasai, H., 2016. Drug Release is Determined by the Chain Length of Fatty Acid-Conjugated Anticancer Agent as One Component of Nano-Prodrug. Bull. Chem. Soc. Jpn. 89 (5), 540–545. https://doi.org/10.1246/BCSJ.20150405.

Kuentz, M., Holm, R., Kronseder, C., Saal, C., Griffin, B.T., 2021. Rational Selection of Bio-Enabling Oral Drug Formulations – A PEARRL Commentary. J. Pharm. Sci. 110 (5), 1921–1930. https://doi.org/10.1016/J.XPHS.2021.02.004.

Li, S., Abdelquader, M.M., Andrews, G.P., Jones, D.S., 2024. Towards a greater understanding of the deep eutectic phenomenon through examination of the lidocaine-NSAID therapeutic deep eutectic systems. Eur. J. Pharm. Biopharm. 200, 114329. https://doi.org/10.1016/J.EJPB.2024.114329.

Li, Z., Lee, P.I., 2016. Investigation on drug solubility enhancement using deep eutectic solvents and their derivatives. Int. J. Pharm. 505 (1–2), 283–288. https://doi.org/10.1016/J.IJPHARM.2016.04.018.

Lu, C., Cao, J., Wang, N., Su, E., 2016. Significantly improving the solubility of non-steroidal anti-inflammatory drugs in deep eutectic solvents for potential non-aqueous liquid administration. MedChemComm 7 (5), 955–959. https://doi.org/10.1039/C5MD00551E.

Macário, I.P.E., Ventura, S.P.M., Pereira, J.L., Gonçalves, A.M.M., Coutinho, J.A.P., Gonçalves, F.J.M., 2018. The antagonist and synergist potential of cholinium-based deep eutectic solvents. Ecotoxicol. Environ. Saf. 165, 597–602. https://doi.org/10.1016/J.ECOENV.2018.09.027.

Marques, M., 2004. Dissolution media simulating fasted and fed states. Dissolut. Technol. 11 (2), 16. https://doi.org/10.14227/DT110204P16.

Martins, M.A.R., Pinho, S.P., Coutinho, J.A.P., 2019. Insights into the Nature of Eutectic and Deep Eutectic Mixtures. J. Solution Chem. 48 (7), 962–982. https://doi.org/10.1007/s10953-018-0793-1.

McMurry, John. (2015). Organic chemistry with biological applications. https://www.stakbogladen.dk/pensumlister/kemi-og-fodevareteknologi/2-semester/isbn-nd-9781285842912-organic-chemistry-with-biological-applications.

Morrison, H.G., Sun, C.C., Neervannan, S., 2009. Characterization of thermal behavior of deep eutectic solvents and their potential as drug solubilization vehicles. Int. J. Pharm. 378 (1–2), 136–139. https://doi.org/10.1016/J.IJPHARM.2009.05.039.

Mu, T., Rarey, J., Gmehling, J., 2007. Performance of COSMO-RS with Sigma Profiles from Different Model Chemistries. Ind. Eng. Chem. Res. 46 (20), 6612–6629. https://doi.org/10.1021/IE0702126.

Mullins, E., Liu, Y.A., Ghaderi, A., Fast, S.D., 2008. Sigma Profile Database for Predicting Solid Solubility in Pure and Mixed Solvent Mixtures for Organic Pharmacological Compounds with COSMO-Based Thermodynamic Methods. Industrial and Engineering Chemistry Research 47 (5), 1707–1725. https://doi.org/10.1021/IE0711022.

O'Shea, J.P., Holm, R., O'Driscoll, C.M., Griffin, B.T., 2019. Food for thought: formulating away the food effect – a PEARRL review. J. Pharm. Pharmacol. 71 (4), 510–535. https://doi.org/10.1111/JPHP.12957.

Oyoun, F., Toncheva, A., Henríquez, L.C., Grougnet, R., Laoutid, F., Mignet, N., Alhareth, K., Corvis, Y., 2023. Deep Eutectic Solvents: An Eco-friendly Design for Drug Engineering. ChemSusChem 16 (20), e202300669. https://doi.org/10.1002/CSSC.202300669.

Paiva, A., Craveiro, R., Aroso, I., Martins, M., Reis, R.L., Duarte, A.R.C., 2014. Natural deep eutectic solvents - Solvents for the 21st century. ACS Sustain. Chem. Eng. 2 (5), 1063–1071. https://doi.org/10.1021/SC500096J/ASSET/IMAGES/MEDIUM/SC-2014-00096J_0010.GIF.

Palmelund, H., Andersson, M.P., Asgreen, C.J., Boyd, B.J., Rantanen, J., Löbmann, K., 2019. Tailor-made solvents for pharmaceutical use? Experimental and computational approach for determining solubility in deep eutectic solvents (DES). Int. J. Pharmaceut.: X 1, 100034. https://doi.org/10.1016/J.IJPX.2019.100034.

Palmelund, H., Eriksen, J.B., Bauer-Brandl, A., Rantanen, J., Löbmann, K., 2021a. Enabling formulations of aprepitant: in vitro and in vivo comparison of nanocrystalline, amorphous and deep eutectic solvent based formulations. Int. J. Pharmaceut.: X 3, 100083. https://doi.org/10.1016/J.IJPX.2021.100083.

Palmelund, H., Rantanen, J., Löbmann, K., 2021b. Deliquescence Behavior of Deep Eutectic Solvents. Appl. Sci. 11, 1601. https://doi.org/10.3390/app11041601.

Panbachi, S., Beranek, J., Kuentz, M., 2023. Polymer-embedded deep eutectic solvents (PEDES) as a novel bio-enabling formulation approach. Eur. J. Pharm. Sci. 186, 106463. https://doi.org/10.1016/J.EJPS.2023.106463.

Panbachi, S., Beranek, J., Kuentz, M., 2024. Hydrophobic deep eutectic solvent (HDES) as oil phase in lipid-based drug formulations. Int. J. Pharm. 661, 124418. https://doi.org/10.1016/J.IJPHARM.2024.124418.

Pereira, C. V., Silva, J. M., Rodrigues, L., Reis, R. L., Paiva, A., Duarte, A. R. C., & Matias, A. (2019). Unveil the Anticancer Potential of Limomene Based Therapeutic Deep Eutectic Solvents. Scientific Reports 2019 9:1, 9(1), 1–11. DOI: 10.1038/s41598-019-51472-7.

Pereira, J., Miguel Castro, M., Santos, F., Rita Jesus, A., Paiva, A., Oliveira, F., Duarte, A. R.C., 2022. Selective terpene based therapeutic deep eutectic systems against colorectal cancer. European Journal of Pharmaceutics and Biopharmaceutics 175, 13–26. https://doi.org/10.1016/J.EJPB.2022.04.008.

Porter, C.J.H., Pouton, C.W., Cuine, J.F., Charman, W.N., 2008. Enhancing intestinal drug solubilisation using lipid-based delivery systems. Adv. Drug Deliv. Rev. 60 (6), 673–691. https://doi.org/10.1016/J.ADDR.2007.10.014.

Pouton, C.W., 2006. Formulation of poorly water-soluble drugs for oral administration: Physicochemical and physiological issues and the lipid formulation classification system. Eur. J. Pharm. Sci. 29 (3–4), 278–287. https://doi.org/10.1016/J.EJPS.2006.04.016.

Pouton, C.W., Porter, C.J.H., 2008. Formulation of lipid-based delivery systems for oral administration: Materials, methods and strategies. Adv. Drug Deliv. Rev. 60 (6), 625–637. https://doi.org/10.1016/J.ADDR.2007.10.010.

Prigogine, I., & Defay, R. (1954). Chemical Thermodynamics: Treatise on Thermodynamics Based on Methods of Gibbs and De Donder. In D. H. Everett (Ed.), Chemical Thermodynamics: Vol. I. Longmans Green & Co Ltd. https://archive.org/details/chemicalthermody0000ipri.

Rahman, M.S., Roy, R., Jadhav, B., Hossain, M.N., Halim, M.A., Raynie, D.E., 2021. Formulation, structure, and applications of therapeutic and amino acid-based deep eutectic solvents: An overview. J. Mol. Liq. 321. https://doi.org/10.1016/J.MOLLIQ.2020.114745.

Rowe, R., Sheskey, P., & Quinn, M. E. (1994). Handbook of Pharmaceutical Excipients.

Ryan, C.J., Cheng, M.L., 2013. Abiraterone acetate for the treatment of prostate cancer. Expert Opin. Pharmacother. 14 (1), 91–96. https://doi.org/10.1517/14656566.2013.745852.

Schäfer, A., Huber, C., Ahlrichs, R., 1994. Fully optimized contracted Gaussian basis sets of triple zeta valence quality for atoms Li to Kr. J. Chem. Phys. 100 (8), 5829–5835. https://doi.org/10.1063/1.467146.

Silva, E., Oliveira, F., Silva, J. M., Matias, A., Reis, R. L., & Duarte, A. R. C. (2020). Optimal Design of THEDES Based on Perillyl Alcohol and Ibuprofen. Pharmaceutics 2020, Vol. 12, Page 1121, 12(11), 1121. DOI: 10.3390/PHARMACEUTICS12111121.

Solymosi, T., Tóth, F., Orosz, J., Basa-Dénes, O., Angi, R., Jordán, T., Ötvös, Z., Glavinas, H., 2018. Solubility Measurements at 296 and 310 K and Physicochemical Characterization of Abiraterone and Abiraterone Acetate. J. Chem. Eng. Data 63 (12), 4453–4458. https://doi.org/10.1021/ACS.JCED.8B00566/ASSET/IMAGES/MEDIUM/JE-2018-005669_0008.GIF.

Sun, X., Pradeepkumar, P., Rajendran, N. K., Shakila, H., Houreld, N. N., Al Farraj, D. A., Elnahas, Y. M., Elumalai, N., & Rajan, M. (2020). Natural deep eutectic solvent supported targeted solid-liquid polymer carrier for breast cancer therapy †. DOI: 10.1039/d0ra03790g.

Suzuki, T., Hara, N., Osa, M., Misawa, K., Imai, K., Fujikura, Y., Maeda, T., Sonehara, W., & Kawana, A. (2017). Efficacy of switching to dolutegravir plus rilpivirine, the small-tablet regimen, in patients with dysphagia: two case reports. Journal of Pharmaceutical Health Care and Sciences 2017 3:1, 3(1), 1–5. DOI: 10.1186/S40780-017-0093-8.

Umerska, A., Bialek, K., Zotova, J., Skotnicki, M., Tajber, L., 2020. Anticrystal engineering of ketoprofen and ester local anesthetics: Ionic liquids or deep eutectic mixtures? Pharmaceutics 12 (4). https://doi.org/10.3390/PHARMACEUTICS12040368.

Vallet, T., Michelon, H., Orlu, M., Jani, Y., Leglise, P., Laribe-Caget, S., Piccoli, M., Fur, A. Le, Liu, F., Ruiz, F., & Boudy, V. (2020). Acceptability in the Older Population: The Importance of an Appropriate Tablet Size. Pharmaceutics 2020, Vol. 12, Page 746, 12(8), 746. DOI: 10.3390/PHARMACEUTICS12080746.

Wang, T.Y., Liu, M., Portincasa, P., Wang, D.Q.H., 2013. New insights into the molecular mechanism of intestinal fatty acid absorption. Eur. J. Clin. Invest. 43 (11), 1203–1223. https://doi.org/10.1111/ECI.12161.

Wang, Q., Wen, H., Wang, Y., Li, Z., Hao, J., Wei, L., Zhai, S., Xiao, Z., An, Q., 2024. Pyridine derivatives as hydrogen bond acceptors to prepare deep eutectic solvents for ammonia storage. Int. J. Hydrogen Energy 50, 1489–1501. https://doi.org/10.1016/J.IJHYDENE.2023.10.017.

Wolbert, F., Brandenbusch, C., Sadowski, G., 2019. Selecting Excipients Forming Therapeutic Deep Eutectic Systems-A Mechanistic Approach. Mol. Pharm. 16. https://doi.org/10.1021/acs.molpharmaceut.9b00336.

Zhao, X., Xu, Z., & Li, H. (2017). NSAIDs Use and Reduced Metastasis in Cancer Patients: results from a meta-analysis. Scientific Reports 2017 7:1, 7(1), 1–7. DOI: 10.1038/s41598-017-01644-0.